Elasticity, multi-phase flow and geophysical pattern formation

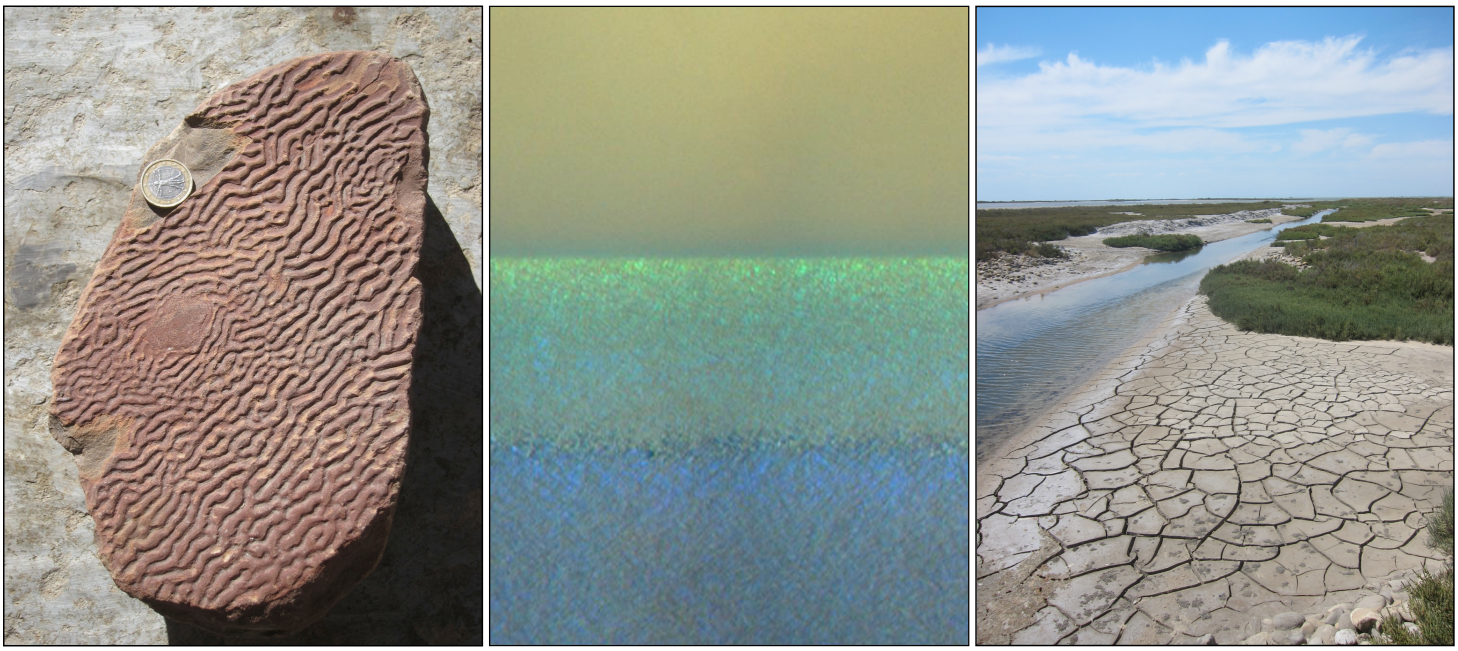

Lucas Goehring

Contents

I. PREFACE

This thesis presents a collection of my research work over the past six years, largely drawn from my contributions since starting a position as a research group leader at the Max Planck Institute for Dynamics and Self-Organization, in Göttingen, Germany, in 2011. As a forward to a cumulative thesis, a general introduction to my work is followed by a number of short sections where the common motivation, physical models and ideas behind my approach to elasticity and multi-phase flow are provided. The collected works are then briefly summarised, and set into context.

The majority of this thesis is a collection of my published works, which relate to my research into a variety of elastic instabilities in multiphase materials. This consists of thirteen peer-reviewed papers [1–13] including three single-authored pieces, and two invited opinion articles. In all but two papers, I am primary author (first/last authorship). For the two works included where I am a secondary author, I contributed to the work of the droplet-stress experiments on colloids of different sizes [7], and the neutron scattering aspects of a study of the mechanisms for locomotion of self-propelled emulsion droplets [12].

Rather than including my works in chronological order, they are instead arranged thematically. First, I include the two opinion pieces, one written on the request of Physics Today, the monthly trade journal of the American Institute of Physics, the other prepared while acting as special editor for a theme issue of the Philosophical Transactions of the Royal Society A, the world's oldest peer-reviewed scientific journal. These introduce a major research focus for me – how geological patterns can be modelled in a physics lab, through the use of analogue experiments. They are therefore followed by three pieces which put these ideas into practice, and where I present work on permafrost patterns, evolving crack networks, and enigmatic fossil wrinkle-structures. From here, I turn to looking at fracture from a more fundamental perspective, and include three further papers which discuss the origins of crack patterns in drying films. Next, I present my work on structure formation in colloidal dispersions. These papers discuss the ordering and disordering of colloidal particles, as they pass from a liquid-like state, to a solid-like state. Finally, two further papers apply some of the above methods in other areas, of self-propelled particles, and cracking starch.

Furthermore, over the past year I have had the opportunity to coauthor a specialist textbook on *Desiccation Fracture and its Patterns* [14], contributing both the general introduction chapters of this book (roughly, the first half), and to certain special topics related to my area of research. As such, certain of the more didactic material (in particular, Sections II and IV) of the introduction of this thesis draw on the text I wrote for this book. For the purposes of inspection, a proof of this book can be downloaded from https://www.dropbox.com/s/jun9wlgpl567zl4/Goehring_book_preprint.pdf?dl=0. The author contributions are clearly identified in the preface to that work, and I use material here only from the text which I was responsible for writing.

II. MOTIVATION: WHY STUDY CRACKING MUD AND DRYING PAINT?

What do a broken-up mud puddle, patterned ground on Mars, and the scales on a Nile crocodile have in common? They are all examples of ordered patterns of cracks, as demonstrated in Fig. 1. Understanding how such patterns form can impact many disparate fields, such as also plant biology (leaf vein development is thought to be possibly initiated by a crack-like instability [15, 16]) and forensics (cracks in dried blood splatter can reveal conditions at the time of death [17, 18]). Further, the ability to control crack formation is important for engineering applications, such as customising novel surfaces [19].

Drying mud occupies a central place to this work. Why mud? Why drying? This is not simply whimsy, but rather reflects the value of desiccation fracture as a simple reliable model for investigating fracture patterns in general. Contraction cracks may be the result of many distinct processes: drying, cooling, syneresis, stretching of a substrate, or differential growth of biological tissue, to give a few examples. However, to a large degree, once the geometry and stress state of a system is set one does not need to know which of these is the driving force, in order to understand the resulting crack patterns. For the particular cases of drying and cooling the connection is even stronger, as there is an exact mathematical analogy between the flow and action of heat and moisture in elastic systems [21, 22]. Moisture is often easier to work with, especially when extreme temperatures are involved. Finally, the

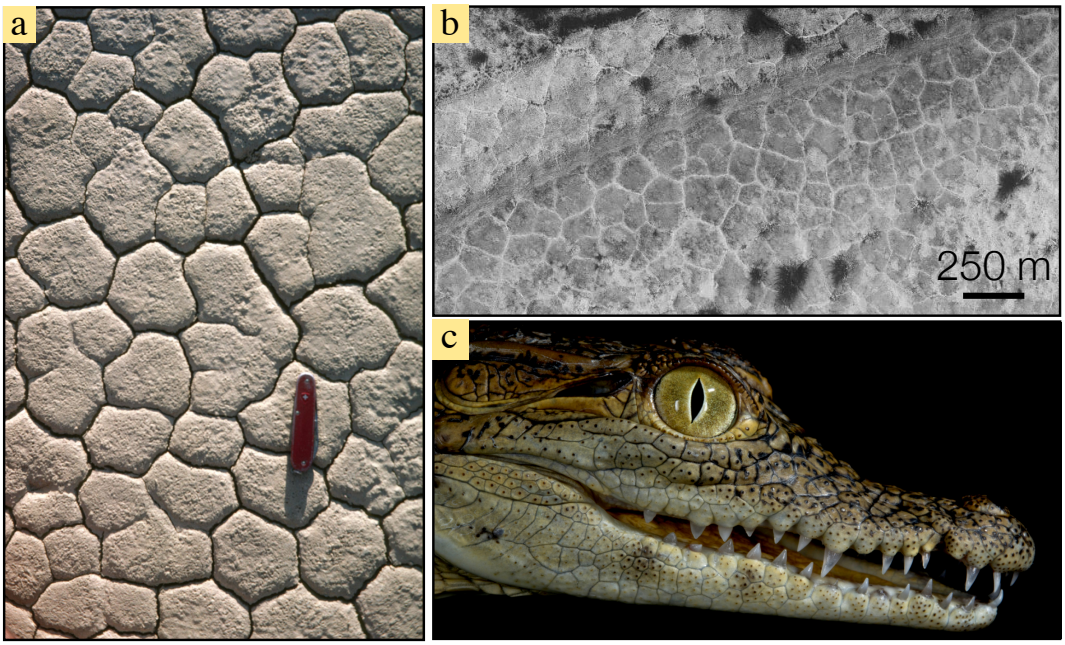

FIG. 1: Mud cracks in Death Valley (courtesy of B. Hallet), permafrost patterns on Mars (Copyright NASA/JPL/Malin Space Science Systems), and the head scales of a Nile Crocodile (courtesy of M. Milinkovitch, [20]). Figure adapted from [1].

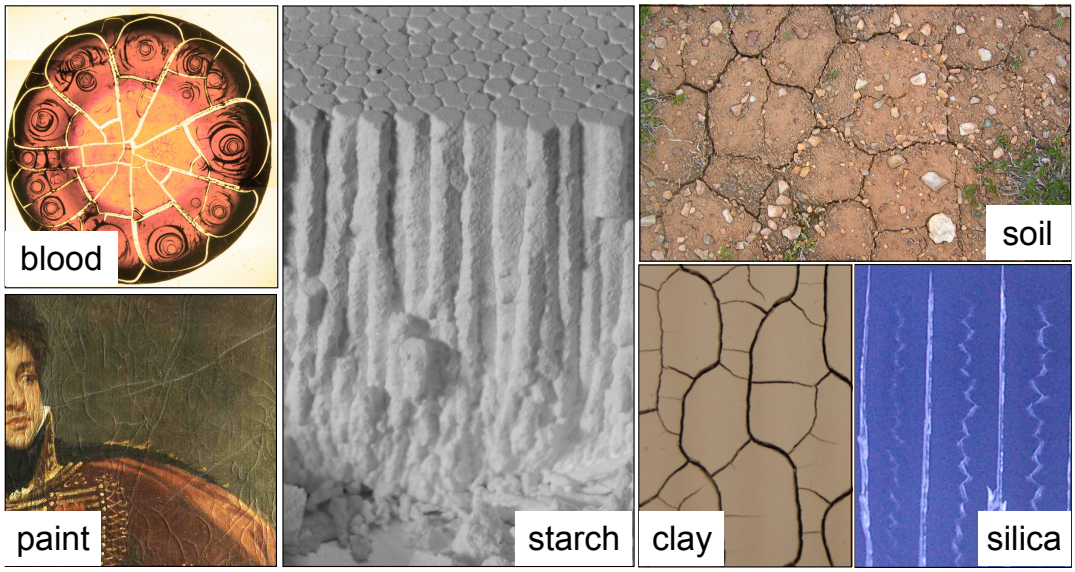

FIG. 2: Examples of desiccation cracking in different media, and under different conditions. Desiccation crack patterns are very rich, and can show spirals, stripes, polygons, waves, and columns, for example. Blood droplet image courtesy of David Fairhurst; paint craquelure image courtesy of Ludovic Pauchard. Figure adapted from [14].

types of patterns that can be found are very rich, and a few example of these are shown in Fig. 2.

A practical approach to studying desiccation cracks can also be useful in two very different ways, either to prevent cracks, or to make use of them. The objective may be to prevent cracks, which is the more traditional objective. But the scientist may also work in a positive sense to produce specific crack patterns for technological applications or to use cracks as a diagnostic tool that gives information about the composition of the cracking material, or ambient conditions which caused cracks. Some demonstrated applications of the study of desiccation fracture include:

- **Industrial coatings.** There is a great interest in replacing paint solvents with environmentally friendly alternatives. These often lead to an increased tendency to crack, during drying, and much work has attempted to prevent this (see *e.g.* a recent review in [23]). Other industrial applications involve the colloidal films that are used as coatings on papers, for ink-jet printing, and for modern high-performance ceramics (*e.g.* turbine blades in jet engines).

- **Photonics.** The manufacture of colloidal crystals, artificial opals, and photonic materials often involves the preparation of a desired structure which is dispersed in fluid, and the fixing of this structure by drying it out. Desiccation cracking is a notorious problem which limits the size of many photonic devices [24–26].

- **Geophysics.** Analogue experiments in geology can allow quantitative access to phenomena which occurred long ago in the Earth's past, on other planets, or over timescales inaccessible to humans. For example, dried starch columns are exact analogues of the columnar jointing of lava [27, 28], while the cracks that form in mud as it is repeatedly wetted and dried can help describe the millennia-long evolution of polygonal terrain in permafrost [4, 5].

- **Biophysical fracture.** Insight from desiccation crack networks has been applied to show that the head scales of the Nile Crocodile develop as a fracture pattern [20], and to explain the ridges on the skin of cantaloupe [29]. There is also a now long-standing question as to whether leaf venation patterns are equivalent to desiccation crack patterns [15].

- **Bespoke crack patterns.** Recently it has been suggested that desiccation cracks and patterns may be used as templates for nano-patterning. The memory effect in pastes, whereby a gentle vibration of the paste prior to drying can determine the orientation of the dried crack pattern [30]. Evaporative lithography can also be used to produce textured surfaces by locally varying the drying rate over a colloidal film [31, 32].

- **Forensics and Medicine** The pattern of cracks in dried blood droplets can be used in the diagnosis of illness [33], or to determine the time and conditions (temperature, relative humidity) at which the blood was spilled, for example in a homicide investigation [17]. Additionally, the craquelure pattern in paintings can be used to help determine authenticity, and authorship [34].

Desiccation fracture also allows a probe into the mechanical response of soft materials. Colloids, clays, and polymer films are all relatively complex mixtures. They are very far from the traditional topics of engineering, or materials science, where fracture mechanics was initially developed. Their behaviour also changes from fluid-like to solid-like as they dry, often very rapidly (*e.g.* gelation, aggregation, crystallisation). Many of the topics that I will discuss try to make a connection between the micro-scale physics of interactions between the individual particles in a solid, and the macroscopic behaviour of that solid as it dries and breaks. A few examples are shown in Fig. 3. As the physics of the micro-scale is, for such materials, intermediate between granular and atomic length scales, new concepts often need to be developed in order to make this connection possible.

III. OVERVIEW

Superficially, I study what happens as paint dries, and mud cracks. Colloids, clays, gels and polymer solutions belong to a class of soft materials that are composed of more than one phase of matter, mixed together in a potentially complex arrangement. The properties and

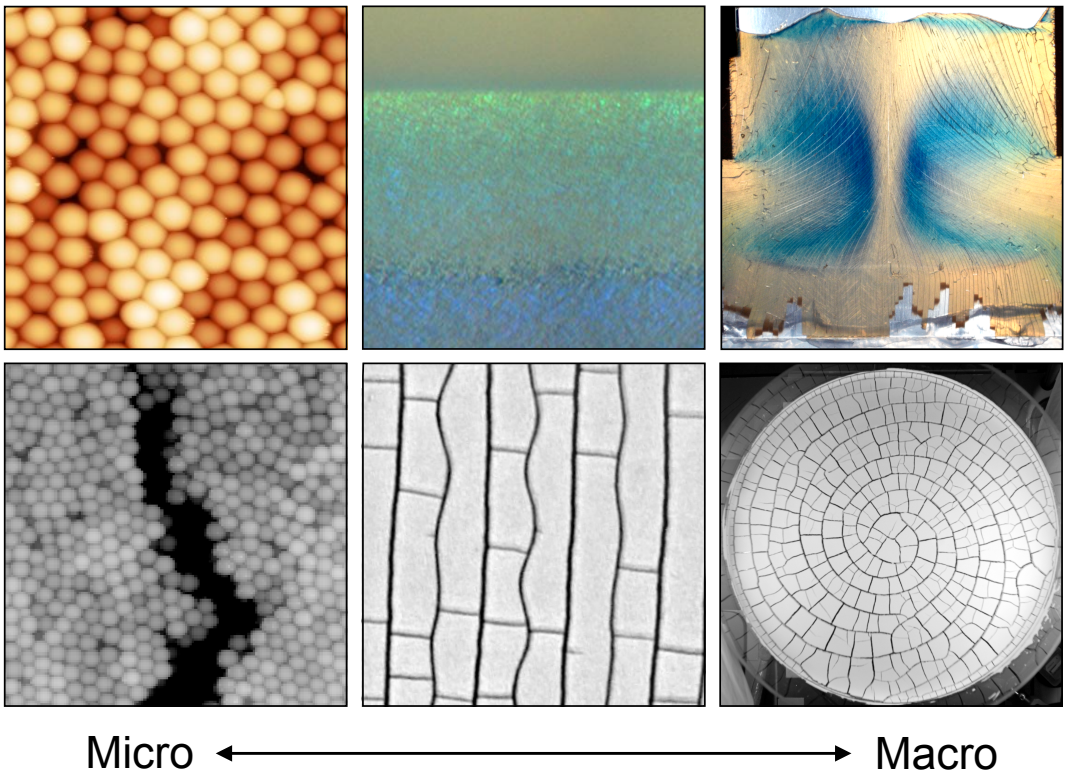

FIG. 3: Drying dynamics from the micro-scale to the macro-scale, and the connection between structure and fracture. In the top row images focus on structural information. From left to right: an atomic force micrograph of dried colloidal spheres; a microscope image of a directionally drying colloidal dispersion, where colour changes reflect changes in structure [9]; and a digital photograph through crossed polarisers showing the pattern of birefringence in a dry film, resulting from anisotropy in the structure [11, 35]. The lower row focuses on the connection to fracture. From left to right: atomic force micrograph of a crack tearing through a drying colloidal film, and causing structural damage [8]; wavy cracks which follow the direction of the drying shown above [6]; and curved cracks which are guided by a structural memory in a paste, induced by vibration prior to drying (panel copyright of A. Nakahara) [30]. Adapted from [14].

dynamics of such mixtures depend intimately on the physics of its different parts, which may consist of a solid-like phase, and a liquid-like phase, and their interactions. More formally, my research looks into a number of instabilities and questions involving elasticity and multi-phase flow in such soft materials. These questions are interdisciplinary, and often take some inspiration from patterns that we can see directly around us, mostly from geological settings. However, some of the questions that have sprung from these origins also involve a mixture of soft matter physics with chemistry, materials science, and biology. What unifies these topics are the methods used – models constructed of strict mass, momentum, and energy balance of the various interacting parts – and the types of fundamental questions asked, which involve the relationship between microscopic dynamics and macroscopic response, as

well as an attempt to understand the types of instabilities that can develop. This thesis summarises my work, over the past six years, of experimental research in this field. Some highlights include:

- The use of sheared polymers to understand the scaling and formation of billion-year old fossil wrinkle structures, which have been a century-old mystery to science [3].
- Modelling of the vast polygonal permafrost patterns of polar Earth and Mars with the cyclic drying of clay in a Petri dish [4, 5].
- The discovery of wavy cracks in thin colloidal films and their use in developing an energy-based model for crack path prediction [6].
- Identification of plastic relaxation mechanisms that can toughen a paint film when, counter-intuitively, the adhesion between its constituent particles is weakened [8].
- Finding a general route of solidification from disordered liquid, to ordered repulsive solid, to an attractive hard solid, as charged colloids dry [9–11].

Although these results are diverse the work here all focusses on the mechanical interactions and responses of multi-phase materials. In the work collected in this thesis three main topics emerge. The first involves the application of laboratory techniques to geophysical problems of pattern formation, where the inhuman timescales or distances involve can make direct field verification of ideas difficult, or impossible. Much of this work, including my earlier studies on columnar joints (which are not included here) turn on fundamental questions of crack growth and propagation in brittle materials. From this, I became interested in the question of how to predict the behaviour of a growing crack, or how a crack interacts with other nearby cracks or an uneven environment. This serves as the second main topic here – the physics of crack interaction and growth in brittle thin films. Or, simply put, how do you predict the path that a crack will take? Finally, as these cracks are driven by the evaporation of water from soft materials, I became interested in the basic problem of how a multi-phase material dries, and solidifies. This has lead to a series of studies on structure formation and the dynamics of drying in soils and colloidal materials (such as the precursors of latex paints).

IV. AN INTRODUCTION TO MULTI-PHASE FLOW

There is an intuitive definition of liquids and solids. Liquids flow, solids do not. In formal terms liquids do not have a shear modulus, at least in the long-time limit. However, a drying material like paint contains at least two phases: an evaporating liquid, and a particulate solid. It can share the properties of both. Indeed, much of the interesting behaviour of drying lies on the interface between liquid-like, and solid-like responses. This can lead to

birefringence in drying colloids [11, 36], or a memory effect that guides crack paths [30], for example. More complex situations may involve the percolation of two immiscible fluids, the presence of a dissolved salt in the liquid phase, reactive flow, or heterogeneity in the solid phase. As each phase can transmit stress, and responds to it differently, the physics of deformation of a multi-phase system can be considerably more complicated than either that of a simple elastic solid, or a liquid.

In 1941 Biot proposed a theory of how to combine the responses of the fluid and solid phases of a rigid porous body [37]. This theory notes that forces can be transmitted by both a liquid pressure, and by stresses in the solid skeleton of the body. The thermodynamically relevant quantity, the total stress, must therefore be the sum of these respective contributions. This perspective can be formalised in a mass and force balance of multi-phase systems, as the theory of linear poroelasticity. Starting instead from a fluid-like perspective, Kynch first suggested a quantitative theory of sedimentation in 1952 [38]. It balanced hydrodynamic drag of a fluid against the gravitational acceleration of sedimenting particles. This notably explained why there can be a shock front in a settling sediment – such as the abrupt line seen in the concentration of cocoa in hot chocolate that has sat for a few minutes.

Within the last decade these two limits have been unified in a more general theory of the solid-liquid transition of multi-phase materials. Work on this has progressed from different perspectives, such as solidification by drying [9–11, 23], freezing [39–41], and filtration [42]. All these diverse phenomena can be captured by considering mass and momentum balances of mixed solid and liquid phases, and the manner in which momentum transfer occurs between phases, through drag. As a short demonstration of these models I will show here that from a mass and momentum balance of the two phases one can derive the Brownian motion of isolated particles in one limit, and Darcy's law of porous medium flow in another. To begin we need to define the relevant stresses and pressures.

The simplest situation is that of a liquid solution or dispersion, containing a solvent/dispersant and a solute/dispersed phase, respectively. The presentation here will be restricted to a mixture such as paint or a clay slurry, composed of small solid particles and a simple liquid, although the ideas can be developed more generally (see *e.g.* [39, 43]). This is, essentially, a modern form of the sedimentation theory begun by Kynch [38].

Start with a glass containing a two-phase fluid of solid particles dispersed in water. The thermodynamic pressure, P, of the mixture may be defined as the isothermal derivative of the system's free energy, U_F, with respect to its volume V,

$$P = \left(\frac{\partial U_F}{\partial V}\right)_{N_i,T} \tag{1}$$

at constant particle number N_i for each phase i. This can be derived from a thermodynamic potential, and reflects the fact that pressure and volume (or their tensorial generalisations, stress and strain), are thermodynamic conjugate variables. Here P is simply the pressure

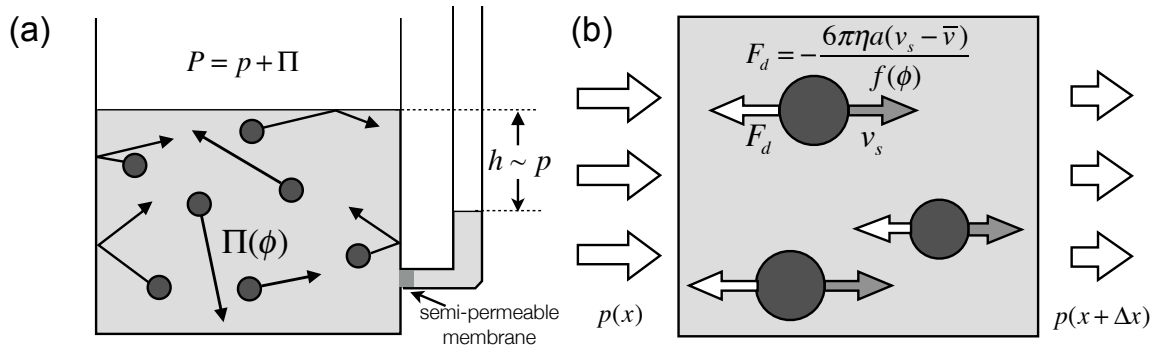

FIG. 4: (a) For a mixture of solid particles dispersed in a liquid, the thermodynamic pressure P of the bulk mixture can be broken down into the sum of the osmotic pressure Π of the solid phase, and the fluid pressure p of the liquid phase. The osmotic pressure can be thought of as the force per unit area of the randomly moving particles bouncing off the walls of a container, while the fluid pressure can be measured by the relative height of a column of pure fluid which is able to exchange fluid molecules with the mixture. (b) If the fluid and particles are moving with respect to each other, the particles feel Stokes drag. On a microscopic scale, there must be a balance between the drag forces felt on all the particles in a volume element, and the change in fluid pressure across that element. Reproduced from [14].

felt on the walls of the glass, or an internal area element.

The particles, or *dispersed phase*, can exert a very different pressure from P, when considered alone. The dispersed particles are thermally active. They randomly hit the walls of the glass with an osmotic pressure Π, as sketched in Fig. 4(a). If the particles are simply an ideal gas of non-interacting points then

$$\Pi = nk_BT \tag{2}$$

where k_B is Boltzmann's constant, T is the temperature and n is the number density of particles. Note that it is often more convenient to work with the solid volume fraction $\phi = V_0 n$, rather than the number density, where V_0 is the average volume of any particle.

In a real dispersion the osmotic pressure tends to be higher than that of an ideal gas, and the effects of particle interactions can be included by defining a compressibility factor $\mathrm{Z}(\phi)$, such that

$$\Pi = \frac{\phi}{V_0} k_B T \mathrm{Z}(\phi). \tag{3}$$

For *stable* dispersions the osmotic pressure must increase monotonically with ϕ. This is equivalent to saying that the bulk modulus associated with the solid phase must be positive.

The water, or *continuous phase*, in the mixture also has its own fluid pressure p (sometimes called the *pervadic* pressure [39, 40]) which can be measured by a manometer. Such a device can be as simple as a long tube attached to the system by a membrane which is water-permeable, but which blocks the particles, as sketched in Fig. 4(a). The height h of pure

fluid that can be supported in this column, relative to the height of the *mixed* fluid in the glass, is proportional to p. If ρ_l is the density of the liquid, and g is the acceleration due to gravity, then equating the fluid pressure at the air-fluid interfaces in the glass and manometer gives us $p = \rho_l g h$.

Since Π and p are the relative pressures of each phase, which can act on an arbitrary surface in or bounding the dispersion, the thermodynamic pressure P of their mixture is

$$P = p + \Pi. \tag{4}$$

This pressure can also be called the total pressure. In the example of the glass full of dispersion there was no bulk flow, and hence P was in hydrostatic equilibrium. However, the two phases may still be in motion with respect to each other, for example by sedimentation of the solid phase. If so, the relative motion will cause drag on the particles, transferring momentum from one phase to the other.

The classic example of drag is the case of an isolated sphere of radius a falling at a velocity v_s in a liquid of dynamic viscosity η, with no walls anywhere. The particle experiences a Stokes drag force

$$F_d = -6\pi\eta a v_s. \tag{5}$$

This can be derived by integrating the fluid pressure felt over the surface of the particle in the viscous limit, assuming a no-slip boundary condition on its surface (see *e.g.* [44]). In the case of particles of other shapes it is customary to use the same formula, using it instead to define a as the effective *hydrodynamic* radius of the particle.

Now consider a collection of particles, of volume fraction ϕ, moving on average at a speed v_s, in a dispersion where one also allows for a bulk, or mean, velocity $\bar{v}$. If we distinguish between v_s and an average velocity v_l of the fluid phase, then for an incompressible fluid the different velocities are related by a mass conservation law,

$$\bar{v} = \phi v_s + (1-\phi) v_l. \tag{6}$$

Since there are now many nearby particles, their mutual hydrodynamic interactions can increase the total drag forces. In this case Stokes drag can be generalised by introducing a dimensionless mobility $f(\phi)$ [39, 40], such that

$$F_d(\phi) = -\frac{6\pi\eta a(v_s - v)}{f(\phi)}. \tag{7}$$

The inverse of the mobility is sometimes used for this purpose, and referred to as the hindered settling coefficient [45] or the sedimentation factor [44].

The drag forces on the particles come from interaction with the fluid phase. In the viscous limit that is appropriate for small particles (and small Reynolds numbers) inertial effects

can safely be neglected. A microscopic force balance can thus be made on a small volume element, as shown in 4(b). This involves equating gradients in the fluid pressure, p, with the total drag forces applied to the particles, and any body forces F_l acting on the liquid. Given an average drag F_d per particle,

$$\nabla p = -nF_d + F_l = \frac{6\pi\eta\phi a(v_s - v)}{f(\phi)V_0} + F_l. \tag{8}$$

As an example of a body force, one could include the effects of gravity by setting $F_l = -\rho_l g\hat{z}$, where ρ_l is the density of the liquid phase.

The evolution of the osmotic pressure must balance that of the fluid pressure, such that

$$\nabla\Pi = nF_d + F_s = -\frac{6\pi\eta\phi a(v_s - v)}{f(\phi)V_0} + F_s, \tag{9}$$

where F_s represents any body forces felt by the solid phase. For example, the effects of buoyancy could be included by setting $F_s = -\phi g(\rho_s - \rho_l)\hat{z}$, where ρ_s is the density of the solid phase. The effects of electromagnetic fields could also be introduced as a body force on the solid phase. We can now put all of this back into the global momentum balance and end up with a model of how the two phases couple. Starting with Eq. (4), the gradient of this total pressure can be balanced by any body forces, $F = F_s + F_l$, felt in the mixture. One could in principle include inertial terms as well, but they are usually negligible for small-enough particles. As such, one finds that

$$\nabla P = \nabla p + \nabla\Pi = F. \tag{10}$$

The body forces may be simply due to gravity, in which case $F = -\rho g\hat{z}$ where $\rho = (1 - \phi)\rho_l + \phi\rho_s$. However, since many clays and colloids contain charged particles, electric and magnetic fields can also have interesting effects (see *e.g.* [46–48] for their influence on crack patterns). For the remaining discussion here it is assumed, however, that there are no significant external forces. Using Eqns. (3) and (8) for the osmotic and fluid pressures, respectively, one then finds that

$$\phi(v_s - \bar{v}) + \frac{f(\phi)k_BT}{6\pi\eta a}\nabla(\phi\mathrm{Z}(\phi)) = 0. \tag{11}$$

This is a force balance equation which describes how the solid volume fraction evolves, without reference to the various pressures in the mixture. Combined with Eq. (6), and the continuity equations for the solid phase,

$$\frac{\partial\phi}{\partial t} = -\frac{\partial}{\partial x}\big(\phi v_s\big) \tag{12}$$

and the liquid phase

$$\frac{\partial(1-\phi)}{\partial t} = -\frac{\partial}{\partial x}\big((1-\phi)v_l\big) \tag{13}$$

it gives a closed system of equations which can describe two-phase flow in a mixture of solid and liquid components. This is not a particularly transparent result, and can be highly nonlinear, so we will next look at how it reduces to more familiar behaviour in two appropriate limits.

A. Liquid-like limit: Fick's laws

If there is no net flow (*i.e.* $\bar{v} = 0$), no body forces, but a concentration gradient in ϕ, then Eq. (11) predicts that the solid particles will move diffusively. Making use of the chain rule, $\nabla(\phi \mathrm{Z}) = (\partial\phi \mathrm{Z}/\partial\phi)\nabla\phi$, gives the solid volume flux

$$\phi v_s = -D(\phi)\nabla\phi \tag{14}$$

for a diffusivity $D(\phi)$. This is Fick's first law of diffusion, which says that the mass flux of a diffusing material is proportional to its concentration gradient. By introducing this result into the solid mass conservation law, Eq. (12), one finds a concentration diffusion equation

$$\frac{\partial\phi}{\partial t} = \nabla\cdot\big(D(\phi)\nabla\phi\big). \tag{15}$$

This is Fick's second law of diffusion. However, the multi-phase flow model also predicts a value for the concentration diffusivity,

$$D(\phi) = \frac{f(\phi)k_BT}{6\pi\eta a}\frac{\partial(\phi \mathrm{Z}(\phi))}{\partial\phi}. \tag{16}$$

This reduces to the case of the Stokes-Einstein diffusivity, $D_0 = k_BT/6\pi\eta a$, in the dilute limit where $f = \mathrm{Z} = 1$.

B. Rigid-body limit: Darcy's law

In the case where the solid phase is stationary, $v_s = 0$, for example in a filter cake, sediment layer or porous rock, then Eq. (8) simplifies to Darcy's law

$$\nabla p = -\frac{\eta}{\kappa}\bar{v}. \tag{17}$$

In this context, $\bar{v}$ is often called the superficial fluid velocity (volume flux per unit area), and p is usually called the *pore* pressure. The resistance of the porous body to flow is given by the *permeability* κ. This model, for spherical particles where $V_0 = (4/3)\pi a^3$, makes a

prediction for the permeability of

$$\kappa = \frac{2a^2 f(\phi)}{9\phi}. \tag{18}$$

While this has the correct scaling (which can be estimated simply on dimensional grounds), there are more sophisticated models of the permeability, such as the Carman-Kozeny equation [49–51], which better account for the complex geometry of a dense pore space. Darcy's law describes the pressure drop of a fluid passing through a porous medium, due to the drag felt on the solid-liquid interfaces. There will, naturally, also be a counter-force that needs to be supported by the rigid skeleton of the porous medium.

C. Network and total stress

The preceding material has explored flow in a multi-phase material composed of a solid phase, and a liquid phase. By breaking the thermodynamic pressure P into separate components for each phase a general model was sketched that is consistent with both Fick's laws of diffusion, and Darcy's law, and which predicts what the diffusivity and permeability appropriate for each situation are. However, so far shear forces have been neglected. The mixture has also been treated as an incompressible fluid, as appropriate for many dispersions, emulsions, or solutions, at least in the dilute limit. When the pressures involved become large enough the elastic response of the component materials can become important. Furthermore, if the solid phase becomes concentrated enough to form a connected network, it can also transmit stress non-isotropically. This need not require particularly high volume fractions: Laponite clay, for example, consists of platelets that gel into a rigid 'house-of-cards' structure at solid volume fractions of only a few percent [52].

In order to include solid-like responses of the two-phase mixture the pressure balance of Eq. (4) can be generalized by introducing a network stress $\tilde{\sigma}$ in the place of the osmotic pressure Π. The thermodynamic pressure P is then naturally replaced by its tensorial form, the total stress σ, and

$$\sigma_{ij} = \tilde{\sigma}_{ij} - \alpha p \delta_{ij}. \tag{19}$$

The negative sign on the pore pressure p reflects the different sign conventions for stress and pressure: a positive stress indicates tension, while a positive pressure is compressive. Here also there has appeared an additional factor α. This is necessary to account for the *relative* compression of each of the two phases, with respect to each other. For incompressible materials $\alpha = 1$, and the simpler balance of Eq. (4) is recovered. Combined with Darcy's law, Eq. (17), and appropriate constitutive relationships for the network and fluid, this division of total stress into an effective stress and a pore pressure is the starting point for considering the deformation of a porous body in the theory of poroelasticity.

D. Poroelasticity and thermoelasticity

For an elastic body an internal pore fluid acts like heat [21, 22]. A constitutive relation for an elastic theory, incorporating either a pore fluid (poroelasticity) or the flow of heat (thermoelasticity), can be derived from the choice of an appropriate thermodynamic potential. However, as the details can be somewhat involved, and the aim here will be to show the analogous manner in which heat and pore fluid can lead to stress. Either case involves an extra two moduli to be defined, in addition to the more familiar elastic moduli (such as the bulk modulus, K). To account for the action of heat, one needs to define a specific heat, c_v, which describes how much the internal temperature will rise, with an injection of heat (here, at constant volume). To couple this to a mechanical response the coefficient of thermal expansion, α_T, is also needed. For a linear response, stress equilibrium is then

$$\nabla \cdot \sigma = \alpha_v K \nabla T \tag{20}$$

where T is the temperature. This is, itself, a diffusive property, which should evolve as

$$\kappa_T \nabla^2 T = \rho c_v \frac{\partial T}{\partial t} + \alpha_v K T_0 \frac{\partial \epsilon_{ii}}{\partial t}. \tag{21}$$

where κ_T is thermal conductivity and ρ the density of the solid. The final term in Eq. (21) is usually negligibly small, and often neglected, but accounts for the change in temperature as a body is compressed, or expanded, adiabatically.

The equivalent theory for poroelasticity first involves taking the divergence of Eq. (19), to give

$$\nabla \cdot \tilde{\sigma} = \alpha \nabla p \tag{22}$$

since, internally, the condition for stress equilibrium is that $\nabla \cdot \sigma = 0$, assuming that there are no body forces. To account for the action of the pore fluid, one needs to additionally define a *specific storage*, M_ϵ, which describes how much the internal pressure will rise, with an injection of pore fluid (here, at constant total system volume). When this is done, one finds a diffusion equation for pore pressure,

$$\frac{\kappa}{\eta} \nabla^2 p = \frac{1}{M_\epsilon} \frac{\partial p}{\partial t} + \alpha \frac{\partial \epsilon_{ii}}{\partial t} \tag{23}$$

which resembles the diffusion equation for the internal temperature of a cooling body. This exact correspondence between thermoelasticity (Eqs. (20) and (21)) and poroelasticity (Eqs. (22) and (23)) allows results obtained in one domain to be applied, directly, in the other.

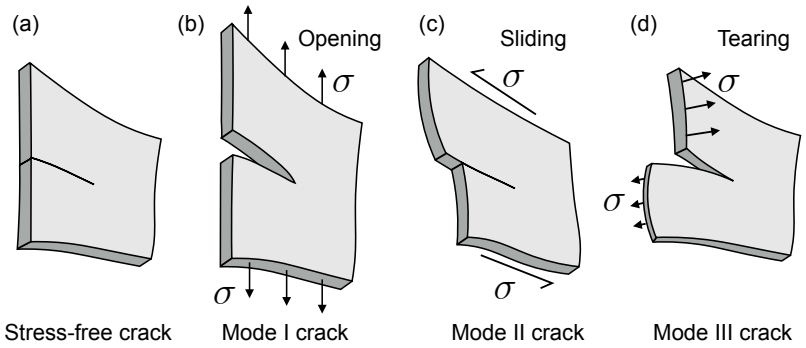

FIG. 5: (a) A crack in a semi-infinite plate, in plane elasticity. The three modes of cracking, (b) opening, (c) sliding (or shearing) and (d) tearing, correspond to the three linearly independent directions that forces can be applied to the crack face. Mixed-mode fracture occurs when more than one mode of cracking is active at the same time. Adapted from [14].

E. Fracture criteria

Poroelastic or thermoelastic stresses can lead to fracture, and this section will therefore end with a short outline of the critical conditions for cracking. The theory of fracture mechanics is centred around the question of when something will break. As shown in Fig. 5, there are three linearly independent modes of fracture, which correspond to different directions over which forces can act on a crack tip. For any mode of fracture cracks will grow when doing so reduces the free energy, U_F, of a system: a crack of some area A grows if $\partial U_F/\partial A < 0$. The *critical point* that distinguishes a situation of a growing crack from one where a crack can exist indefinitely occurs when there a change in the sign of the energy release rate. The crack becomes unstable when

$$\frac{\partial U_F}{\partial A} = 0 \quad \text{and} \quad \frac{\partial^2 U_F}{\partial A^2} < 0. \tag{24}$$

Despite the importance often given to the first constraint, both conditions are necessary in order to distinguish between stable and unstable cracks. For example, a thermal gradient [53], or a gradient in the pore pressure of a drying material [28, 54], can stabilise a crack and halt its growth from a region of high stress, to a region of low stress.

By dividing up the total energy into the energy stored internally in the deformation of the body – the strain energy, U_s – and a surface energy, one can reframe the critical condition for fracture propagation in terms of the strain energy release rate $G = -\partial U_s/\partial A$. This form is known as Griffith's criteria for fracture propagation,

$$G = G_c \quad \text{and} \quad \frac{\partial G}{\partial A} > 0 \tag{25}$$

where the critical strain energy release rate G_c is the energy cost to extend the fracture. For

a thermodynamically reversible system G_c is equal to the interfacial energy of the breaking material, or twice its surface energy [55]. Irreversible energy costs can also be included in G_c, but this can require some caution [56]. For a linear elastic material the strain energy density typically scales as $U_s \sim \sigma^2/E$, where E is Young's modulus, and σ is the stress tensor. The strain energy release rate will therefore scale as

$$G = c^2 \frac{a\sigma_0^2}{E} \tag{26}$$

for some characteristic length-scale a of a crack, characteristic applied stress σ_0, and a pre-factor c that depends on the specific geometry of the system.

Finally, by considering the manner in which stresses are concentrated around a sharp point one can demonstrate that there is a universal divergence of stress near a crack tip [57]. In Irwin's reformulation [58] of Griffith's fracture criterion, the intensity of this divergence is called the stress intensity factor K. It can be linked directly to the strain energy release rate by considering the displacements and surface tractions along the surface of an open crack. For example, given an opening (mode-I) crack,

$$K_I = \sqrt{GE} = c\sigma_0\sqrt{a}. \tag{27}$$

Similarly, for shearing (mode-II) and tearing (mode-III) stresses, one can define K_{II} an K_{III}, respectively. In Irwin's stress-representation, the critical condition for fracture assumes the form

$$K = K_c \quad \text{and} \quad \frac{\partial K}{\partial A} > 0 \tag{28}$$

for some fracture toughness K_c.

V. GEOPHYSICAL PATTERN FORMATION

The Earth is a complex, non-equilibrium, and nonlinear system. These are natural conditions in which to expect self-organisation, which is indeed seen from beach ripples and mega-dunes [59], to rhythmic chemical precipitation [60], branching streams [61], and mud-cracks [5]. These structures usually arise from competition between two opposing forces, and their shapes, sizes, and dynamics contain quantitative information about how they formed, and the mechanisms underlying them. Such patterns can display fascinating order, and can show an amazing robustness, despite a very noisy environment.

The common approach that I have brought to geophysical problems is to identify what the driving mechanism behind a particular geophysical pattern could be, then to simplify this into a dimensionless model, which can be rescaled into a laboratory environment. This rescaling may also involve relying on analogous physics, such as moving from a thermoelastic driving force, for fracture in permafrost soils, to a poroelastic driving force, for fracture in

drying clays [1, 5].

Once a suitable analogue is identified, then an experimental model is constructed in which the scaling theory and onset of instabilities can be tested. In such experiments a similarity of form, no matter how attractive, in insufficient for proof. It is far too easy to generate the limited variety of simple prototypical patterns – waves, hexagons, spots, spirals, *etc.* – by any of a wide variety of different mechanisms. Instead, one must rely on quantitative comparisons, such as the critical conditions for the onset or transition in patterns, the scaling laws for wavelengths or timescales, or the exact values of dimensionless parameters.

Finally, once a model has been tested experimentally, it can be returned for a novel round of verification against direct field measurements. The insight gained from the lab will often suggest new observations that can be made, or guide interpretation of existing data. In these situations, one finds that the mere appearance of patterns in a natural environment can be a powerful diagnostic tool of the processes that happened during their formation, which may be long in the past, or in remote locations, such as Mars or even the polar regions of Earth, which are challenging to access directly.

This general reductionist approach to studying geophysical pattern formation is explained in more detail in [2]. This article was written to introduce a special theme issue, where the tools of pattern formation and nonlinear dynamical systems are applied to geophysical problems. In this issue, reviews on the established topics of dunes [59], coastline morphology [62], submarine channels [63], and Liesegang banding [60], were presented alongside research articles representative of a growing community of interdisciplinary scientists. Despite the obvious appearance of geomorphic patterns, we are only beginning to learn how to read and understand them properly. This issue also shows, for example, how fossil patterns can be used to interpret events far off in time [3], or how patterns seen by satellite imaging can be used to understand the formation of landscapes [64]. Similarly, patterns evolve as conditions change, and the topics discussed there make predictions as to how coastlines [62], marshes [62], deserts [65] or permafrost [5, 66] will change in response to climate change, or can be controlled by human ingenuity.

In my own research I have now followed this paradigm through to explain features of three different physical systems: columnar joints, polygonal terrain, and Kinneyia. An accessible review article of the first two problems is provided here in **??**. The results on columnar joints – the prismatic pillars of basalt that famously pattern landscapes like the Giant's Causeway or the Devil's Tower – was the subject of my earlier work [28, 67–69]. It is referenced occasionally here, in particular in [1, 5], where I show how these patterns can be treated as a special case of a more general pattern-formation process, but is not a significant part of what is presented here. Rather, I will focus on setting into place my research into Kinneyia, fossil wrinkle patterns in ancient biofilms, and on the evolving fracture networks that are responsible for the permafrost patterns already alluded to in Fig. 1.

A. Kinneyia: a fossil enigma, a fossil instability

Kinneyia is a fossil wrinkle pattern found in the fossil record from over half the history of our planet, from the mid-Archean to Jurassic periods [70, 71], but which has been singularly absent from this record for the past 200 million years. It consists of small wrinkles, similar in appearance to beach ripples, but noticeably smaller, as shown in Fig. 6. Typically, these millimetre-to-centimetre wide periodic marks appear in association with shorelines, and usually form as the capping layer of a major storm deposit, or other violent event.

The type fossil *Kinneyia* was catalogued by Walcott, well-known for his pioneering work on Precambrian/Archaean palaeontology, in 1914, and has remained a puzzle for the past hundred years. He suggested that it was the remains of a particular species [72], but the ripple-markings of Kinneyia are now known to be much more generic, and belong to a class of features known collectively as 'microbially mediated sedimentary structures' [71, 73, 74]. In simple terms, Kinneyia is analogous to a footprint left by some kind of activity of ancient microbial mats. However, the mechanism of its formation has remained elusive so far.

In [3] we suggest a simple, robust mechanism to explain the formation of Kinneyia, as the fossilised remains of a hydrodynamical instability in ancient biomats. Modern biofilms and biomats consist of microbes held together by a gel-like matrix of extracellular polymeric substances (see *e.g.* a recent review [75]). The rheology of this matrix is similar to that of a polymer solution, and the mat behaves in many ways as a viscoelastic [75, 76]. Remarkably, despite the fact that biofilms' effective steady-state viscosity and shear modulus vary by many orders of magnitude, across different species, the ratio of these two properties, which defines a relaxation time, is strongly preserved, and typically about 20 minutes [76].

Based on the rheology of modern biomats, and the close association of the respective fossils with storms, we suggest that Kinneyia patterns form by a hydrodynamic instability of the surface of a biomat, when water flows over its surface. This is a Kelvin-Helmholtz type instability, similar to how shear flow in cloud layers can lead to the gentle undulations of the edges of a cloud bank. Generally, the interface between two viscous layers, which respond to shear in different ways, will be unstable under shear flow. We performed a linear stability analysis of a simple geometry consisting of a viscoelastic mat adhered to a rigid substrate, over which water flowed at some fixed speed v. The analysis predicts that the film's surface is unstable to wrinkling on a wavelength about 4-5 times the thickness of the film [3], and that the wavelength does not depend on either the film's viscosity, or the flow speed v (although the growth rate of the instability should depend on both).

Analogue experiments using polymer solutions as mats confirm these predictions – under flowing water ripples spontaneously form at a wavelength 3-4 times the thickness of the film, h, and grow at this wavelength to reach a saturation amplitude $\sim h$. Fossils, and casts of fossils, were also collected from exposures of Kinneyia in Namibia, and scanned to produce a 3-D height profile. The ratio of wavelength to amplitude matches the experimental observations, and while we do not know the thickness of the original mat (as the fossil only

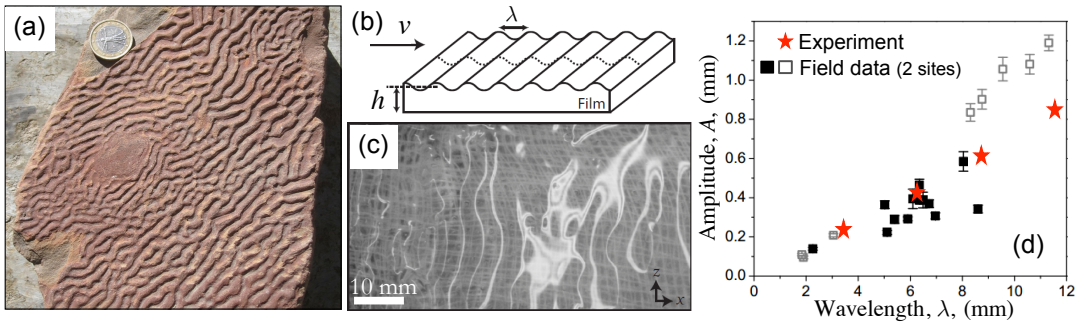

FIG. 6: (a,b) Kinneyia is a wrinkle-pattern found in the fossil record between 2.9 and 0.2 billion years ago. (c) Here it is suggested that it forms by an instability of a thin viscous fluid to the shear flow of water above it. A linear stability analysis [3] suggests that the interface between the two fluids will become unstable to periodic wrinkling. The most unstable mode of the ripples, λ, is predicted to be proportional to the film thickness h, and independent of the flow speed v, or viscosity of the mat. (d) Experiments on analogue fluids, consisting of a 1-4 mm thick layer of cross-linked poly(vinylalchohol) solution, over which water has flowed. The wavelength of the resulting ripples agrees with the predictions of linear stability theory, while (d) the saturation amplitude A agrees with comparable measurements from field specimens. Adapted from [3].

preserves the sediment's imprint of the mat), the thickness inferred from their wavelengths matches those of typical modern mats [3].

The robustness of the wrinkling mechanism suggests that similar structures should be seen in modern mats. However, Kinneyia is linked to storm deposits, which are infrequent. Additionally, grazing animals and rapid bioturbation since the Cambrian have rendered conditions for biomats increasingly unfavourable; they are relatively scarce today. Thus, Kinneyia may have become so rare as to not enter the fossil record. Another line of thought concerns rheology: biomats are living, active matter, capable of a mechanical response to stress.. As we do not know the history of this response, the microbial mats may well have evolved an active motion to counteract the wrinkling instability. We are developing biotic experiments to check these possibilities, either of which would profoundly impact how we interpret these fossil clues to the history of life on Earth.

Finally, although our suggested mechanism for Kinneyia was published less than a year ago, it has already prompted some notable discussion. In particular, another model of wrinkle-formation has been proposed [77], based on the scouring action of broken fragments of mat, floating in wavy water. These two models now make different predictions for the conditions in which Kinneyia should form, and the next round of experiments are already being designed and run in my group.

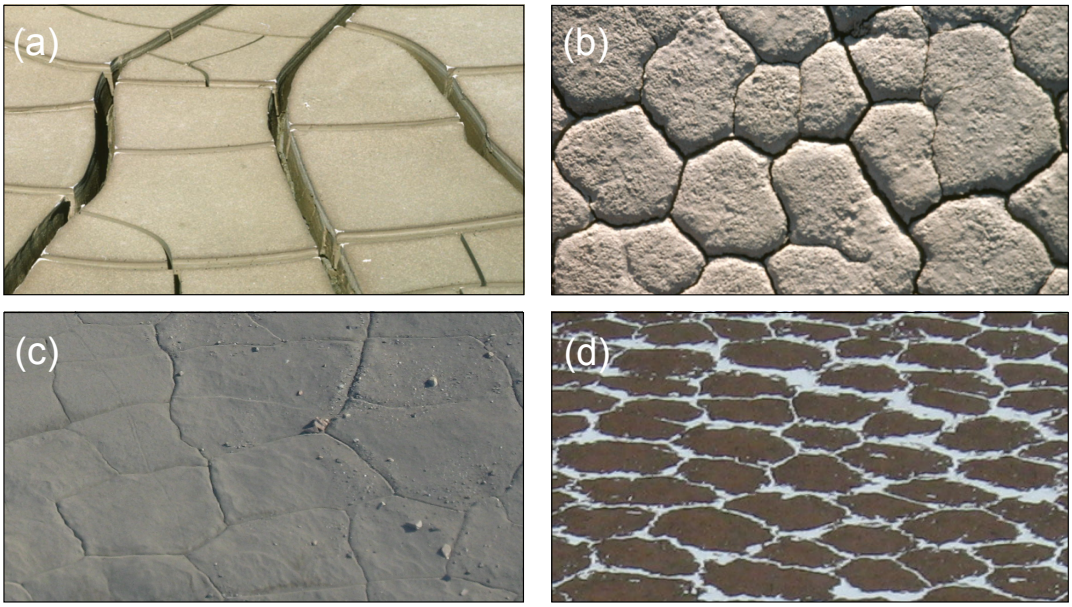

FIG. 7: Cracks in mud can show (a) a rectilinear pattern, or (b) a hexagonal pattern (images courtesy of Bernard Hallet). Cracks in permafrost soils can also form in (c) rectilinear patterns, or (d) hexagonal patterns. Visually, such polygonal terrain looks similar to mud crack patterns, except that the spacing between cracks is much larger, about ten metres. Both mud cracks and polygonal terrain form as the result of the contraction of a 'thin' brittle layer – where the layer thickness is the shortest relevant length-scale in the problem. Adapted from [14].

B. Drying mud and permafrost patterns

What do mud crack patterns look like? In nature, one can find mud cracks with a mostly rectilinear pattern, like that shown in Fig. 7(a). However, as shown in Fig. 7(b), hexagonal mud cracks are also relatively common. They are often seen in places like Death Valley, or near the toes of glaciers, where a fine-grained clay sits undisturbed for long periods of time, except for changes in the weather. In [4, 5] I explored the differences between these two patterns, explained how a rectilinear crack pattern can evolve towards a hexagonal one, and identified the necessary conditions for it to do so.

Similar patterns, on a much different length scale, are also seen in frozen soils in the polar regions of the Earth and Mars. Permafrost occurs in ground where the mean temperature, averaged throughout the year, is below zero. The pore space in permafrost soils is often saturated with ice, and forms into a very tough ice-cemented soil. Despite the average temperature being sub-zero, there are still significant annual temperature swings between summer and winter. The thermal stresses associated with these temperature variations can easily be large enough to open contraction cracks in ice-cemented permafrost soils, a few centimetres wide and a few metres deep, during the winter [78, 79]. These cracks form a network with an average spacing between cracks of about ten or twenty metres. Nevertheless,

the cracking soil can be considered as a 'thin' film, as its thickness is small compared to any other relevant length-scales. Indeed, it was recently shown that the spacing of thermal contraction cracks in Antarctic soils is proportional to the thickness of the ice-cemented soil layer [80]. This is expected for thin layers, due to the effect of crack saturation [81]. During the summer months the ground warms and the cracks close and at least partially heal. However, while they were open, material such as sand or snow will have had the opportunity to fall into the cracks. This intrusive material will act as a line of weakness, guiding the formation of cracks near the same locations, in the following winter. Over tens of thousands of years, this process is known to lead to the complete overturning and recycling of near-surface permafrost soils [82, 83].

The networks of cracks that occur in permafrost regions create vast landscapes, known as polygonal terrain. These cracks are much bigger, and more widely spaced, than the cracks in dried mud, but otherwise closely resemble them. They can also appear as a rectilinear pattern, as shown in Fig. 7(c), or a hexagonal network, as shown in Fig. 7(d). Based on a number of different dating techniques it is known that the hexagonal patterns are usually much older than the rectilinear ones, suggesting that there is a dynamical process linking the two types of network [83]. However, due to the millennial timescales involved, there are only limited direct measurements that can be made on the evolution of polygonal terrain.

The two problems of mud cracks and polygonal terrain are, in fact, related. There is an exact mathematical analogy between the physics of cooling and drying, and the stresses that either develop. This was discussed above in Section IV.D. In particular, both heat and moisture act as diffusive properties. As a result, one can write a diffusion equation for the internal fluid pressure p, or temperature T [21]. This diffusive field is coupled to the stress $\tilde{\sigma}$ in the solid network of soil grains, where the appropriate balance of internal forces gives

$$\nabla \cdot \tilde{\sigma} = \begin{cases} \alpha \nabla p \\ \alpha_v K \nabla T \end{cases} \tag{29}$$

for the cases of stress induced by an uneven pore pressure p or temperature T. In a thin layer where the temperature or pore pressure only varies vertically, the resulting stress will be an in-plane tension of the cooling permafrost soil or drying clay. These tensions will lead to the cracking of the cooling or drying layer, through the process of sequential fragmentation. Cracks form one at a time, run across the mud until they hit another crack, or a boundary, and the crack spacing saturates when it is comparable to the thickness of the cracking layer. For an initially homogeneous layer a later crack will tend to curve to hit an earlier one at right angles, because the earlier crack has already released the stress normal to itself [84]. It has not been clear how the same forces could generate a hexagonal pattern, and [4, 5] set out to answer this question.

Based on the analogy between poroelasticity and thermoelasticity, and on the known

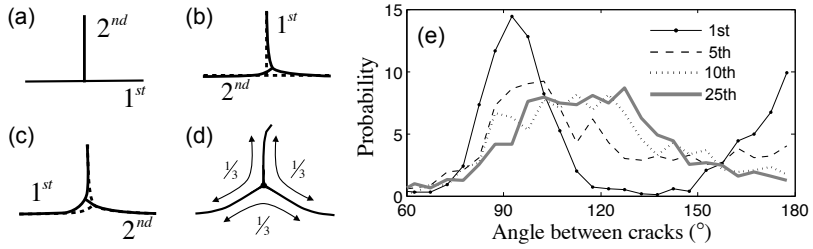

FIG. 8: (a-d) A schematic mechanism for the evolution of a mud-crack pattern, through repeated dryings. (a) In the first cycle of cracking a later crack hits an earlier one at right angles. (b) In the next cycle, if the order of cracking changes, the vertex position will be deflected, as each individual crack will grow in a manner that maximises its strain energy release rate, at the point and time of crack opening. (c) The differences after repeated cracking cycles will accumulate, and (d) distort the vertex until a more stable configuration of equi-angled joints is reached. (e) The distribution of angles between cracks evolves over time: shown here are the probability distributions of the joint angles after the 1st, 5th, 10th, and 25th cycle of cracking. Reproduced from [14].

behaviour of permafrost soils, I developed an analogue experiment to study the dynamics of polygonal terrain [4, 5]. Layers of bentonite clay, a few millimetres thick, were dried. These layers crack, but the cracks heal if the mud is rewet, for example by spraying the clay's surface with a find mist of water until it is saturated. When the mud is dried for a second time it cracks again, and the new cracks form near the lines of the cracks from the first drying [4]. However, there are subtle differences between the cracks in the first, second, and subsequent dryings. The positions of the cracks are nearly the same, but the vertices formed by the intersection of different cracks have shifted slightly, and the angles at which the cracks approach those vertices have changed. This cycling of drying and wetting can be repeated indefinitely, and the differences in the patterns will slowly accumulate, allowing the possibility for the gradual rearrangement of the crack network [4, 5]. The physics of this evolution is explained at length in [5], and sketched here in Fig. 8 (a-d).

The process described above will create a slow, but directed, motion of the vertices. If the clay is rewet and dried for a third time, the cracking can change slightly, again. The effect of this is predicted to be a gradual, ratchet-like motion of the vertex up the crack branch that originally approached the vertex at two right angles [4], which is in experimental mud-crack patterns [5]. Furthermore, the angles around the vertex will stretch and approach 120°. Indeed, averaged over long enough time, if all the possible sequences at which cracks populate a vertex are explored with equal probability, symmetry alone would predict a 'Y' shape to the vertex, with all angles equal, as sketched in Fig. 8(d). The distribution of angles between cracks, at vertices, was measured over the first 25 cycles of cracking [4], and some of these results are shown in Fig. 8(e). The mud-crack pattern evolves from a population of right angled crack junctions, to equi-angled Y junctions, over only a few cycles of cracking and healing.

The essential conditions for the evolution of a crack pattern, in the manner described

above, can be briefly summarised [5]. First, cycles of cracking must occur repeatedly, for example in the cracking/healing manner of the mud-crack experiments, or by advancing through space like columnar joints, in order for there to be any opportunity for evolution. Second, the positions of cracks from previous cracking cycles must guide the locations of any new cracks, but not determine their sequence. If there was no memory then the cracks would be randomly generated in each cycle, while if there was too strict a repetition of the pattern there would be no driving force for change, besides random noise. Finally, the paths of the cracks must be determined, in each repetition, by growth along the direction that maximises the difference between the strain energy release rate G, and the surface energy of the new cracks, G_c. In Section VI this will be introduced as the condition that $G - G_c$ is maximised along the path of crack growth, as an extension of the Griffith criteria.

These conditions apply equally well to mud cracks and to polygonal terrain, whose pattern evolves over thousands of years. The cracks in permafrost reform each winter, and heal each summer. These cracks have a long-term memory, even forming depressions in the ground over thousands of repetitions [78, 83]. The sequence of cracking has been measured using buried electrical cables: when a crack opened it would break a cable running across it, and the time of this could be recorded electronically [79, 85]. The sequence of breaking differs in different winters, giving the pattern the necessary driving force for change.

More generally, these conditions apply to a wide range of interesting patterns, including columnar joints [1, 5], fracture patterns on eroding gypsum dunes [5, 86], and perhaps surprisingly the embryonic development of scales on head of Nile Crocodiles [20], and can explain the appearance of ordered crack patterns in these systems.

Finally, to return to the original question of this section: what do mud crack patterns look like? If they are fresh patterns, forming in homogeneous mud, they will be rectilinear. If the mud is incapable of any memory then the mud-cracks will also be rectilinear, even if the mud is dried and wet repeatedly. If there is memory, either stored in the structure of the mud (as in [30]), or as an imperfectly healed crack surface, or stored geometrically by a permanent depression near the locations of cracks (like in polygonal terrain), then there is the possibility for evolution. If this is the case, and if the mud is allowed to crack and heal many times, then the pattern can evolve towards a hexagonal pattern.

VI. FRACTURE PATTERNS IN THIN FILMS

As has already been suggested above, fracture patterns can be very rich, and represent a challenge to explain. However, their diversity also represents an opportunity – there is no generally accepted model to explain the direction in which a crack will grow or propagate. The physics of these patterns is captured by an energy balance as the cracks grow. Unlike many other physical problems, however, crack growth involves only a local energy minimisation, at the point and time that a crack is growing, rather than the global minimisation of

some functional. Since energy can be released by the widening of a crack anywhere along its path, whereas to a good approximation energy is only spent in a small region immediately around a growing crack tip, the entire history of the crack affects how it will grow at any instant. This means that although the highly practical question of whether a crack will grow or not (and hence, whether a bridge will fall down, or an airplane wing snap off) is solved, one cannot accurately predict, yet, the direction that a crack will grow in any but the simplest cases. I am investigating the dynamics of cracks in thin sheets, with two general long-term goals:

- Predicting how a crack will grow in an arbitrary situation, and
- Designing/templating structures to give a desired crack pattern.

Here I present two main results, which aim towards these ends. First, I will discuss the problem of crack path prediction, and show how wavy cracks appear in drying colloidal films. These are used to start developing a model of how cracks interact with each other, to determine which way they will grow [6]. Second, I will discuss the problem of how to evaluate fracture criteria in thin films that may have a non-linear elastic [7] or plastic [8] response. These relate to how to design crack-resistant films and coatings.

A. Crack paths, interacting cracks, and wavy cracks

The critical conditions for fracture were introduced in Section IV.E, and are a well-established theory with immense practical value in engineering disciplines. However, in order to form a complete theory of fracture these conditions need to be supplemented with an equation of motion for a growing crack tip (see *e.g.* a recent discussion in [87]). The geophysical problems discussed above have already hinted at this need. To date there is no general rule, derivable from first principles, which describes which way a crack will grow.

The lack of a well-founded model for crack path prediction is an area where desiccation/contraction cracks are making fundamental contributions. The development of a rigorous theory, with a wide range of applicability, will require a combination of experimental, numeric, and theoretical efforts on a number of paradigm-systems. Table-top experiments in slurries, pastes, or gels, allow patterns to develop through the interaction of simple individual cracks in thin, approximately 2D layers. They give repeatable results in simple and repeatable conditions, and demonstrate instabilities such as spirals [88, 89], waves [6], starbursts [90, 91] and other structures [92, 93]. They also allow the control of the forces on these cracks through modulation of electric and magnetic fields [46–48]. Such experiments are giving direction, and strict observational constraints, to a search for a general law of crack path selection.

This is not to say that there are not good guiding ideas for crack path prediction. In fact, there are two. First is the extension of the Griffith criteria for fracture, which balances

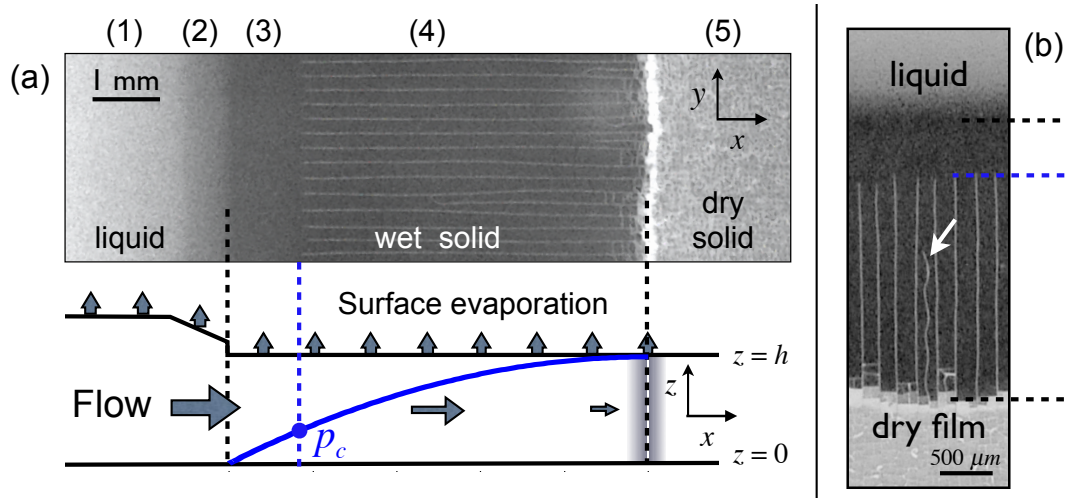

FIG. 9: (a) Directional drying of colloidal dispersions leads to the development of a series of drying fronts. (1) A liquid dispersion like paint first (2) orders, then (3) solidifies [9]. The solid (4) cracks, and ultimately (5) drains of water, forming the final dry solid porous film [97, 98]. The wet solid regions (3-4) are usually modelled as elastic materials, across which extend gradients in capillary pressure, and hence in-plane stress. These gradients are a result of surface evaporation, which drives Darcy flow through the porous film (Eq. (17)). Cracks may grow when the magnitude of the pore pressure (blue curve) reaches some critical value p_c. (b) Wavy cracks can form by growing between the usual array of parallel cracks. Adapted from [6, 8].

the strain energy release rate G with the energy losses during fracture, G_c. In this model, a crack grows in the direction which maximises $G - G_c$, at all points along its path [56]. Although easy to state in words, further development of the variational principles necessary to give the condition of a *maximum energy release rate* quantitative predictive power has proved difficult, for a number of reasons. The energy release rate is hysteretic, in that it can depend on the entire past path of the crack. Furthermore, the mathematics of treating even a slightly curving or kinked crack are already exceptionally challenging [94].

Alternatively, the *principle of local symmetry* predicts that a crack will follow a path where the shear stress intensity factor is zero, $K_{II} = 0$, because otherwise the force distribution around a crack tip would be asymmetric, and this could be expected to bias the growth of the crack towards the direction of higher stresses. For the limit of an isotropic solid under constant loading conditions and plane elasticity the principles of local symmetry and maximum energy release rate are equivalent [94, 95]. For more generic conditions this will not be true. A simple counter-example is if G_c is direction-dependent (*e.g.* cleavage along crystal planes) as K_{II} cannot encode such information. Yet as elegantly demonstrated by recent experiments where wavy cracks in a film are guided by the orientation of a silicon crystal substrate [19], G_c matters to crack paths. An additional case where G_c is important is the memory effect where the anisotropic structure of a paste can guide crack paths along the direction of a remembered vibration, or flow [30, 96].

In [6] I identify how wavy cracks appear in drying colloidal films. In this experiment a thin layer of liquid colloidal dispersion is painted onto a glass slide, and allowed to dry. It does so directionally, from the edges inwards, forming a rigid solid film during the process. The capillary pressures in the film are easily large enough to drive fracture, and here cracks will advance directionally, across the film, following the line of the drying, as sketched in Fig. 9. Normally, a set of equally-spaced out parallel cracks will form, with a crack spacing proportional to the film thickness [51, 99–101]. The tips of these cracks are arranged along a cracking front, parallel to the drying fronts, fixed by some critical cracking pressure p_c.

However, as described in [6], occasionally a crack will form behind this regular cracking front, between two existing straight cracks. The flanking cracks preferentially release stress normal to their surface, and so the wavy crack would gain energy by curving towards either one. However, as it approaches one it must advance into a region with a lower total strain energy density. A balance between these effects suggests an oscillating path, which continuously curves towards the local direction of maximum strain energy release rate.

The geometry of wavy cracks in a thin film is simple enough to permits an analytic test of the crack path models outlined above [6]. The form that a generic equation of motion for a crack could take is severely constrained by symmetry. A framework for this was provided by Hodgdon and Sethna [102]. The goal is to predict the path $\Gamma(l)$, parameterised by some path length l, which a crack tip follows as it grows. In a two-dimensional film the crack tip will have some unit tangent vector $\hat{t} = d\Gamma/dl$ and an accompanying normal vector $\hat{n}$. The motion of the tip, if it grows smoothly, can be fully described by its acceleration

$$\frac{d^2\Gamma}{dl^2} = \frac{d\hat{t}}{dl} = f\hat{n}. \tag{30}$$

The first equality here involves simply taking the derivative of the definition of the tangent vector, with respect to the path length. For the second equality, one notes that $\hat{t}$ is a unit vector, and cannot change its length. It can only be subject to a normal acceleration. As such, it must hold that $d\hat{t}/dl = f\hat{n}$ for some function f. Furthermore, inversion symmetry in the choice of the normal $\hat{n}$ requires f must change sign under the operation $\hat{n} \to -\hat{n}$ (*i.e.* f is a pseudoscalar). Up to this point, this model is only a pure statement of geometry. The choice of f contains all the physics.

For a wavy crack in a thin film adhered to a rigid substrate, the forces acting on the crack tip, and the manner in which it relaxes stress, can be simplified. Here, we formulated the principle of maximum energy release rate by a linearised form for f which includes the term

$$\frac{d^2\Gamma}{dl^2} = -\left(\frac{1}{G_c}\nabla G \cdot \hat{n}\right)\hat{n}. \tag{31}$$

This predicts that an advancing crack always curves up any local gradients in the energy release rate, with a curvature proportional to the magnitude of the gradient. We then

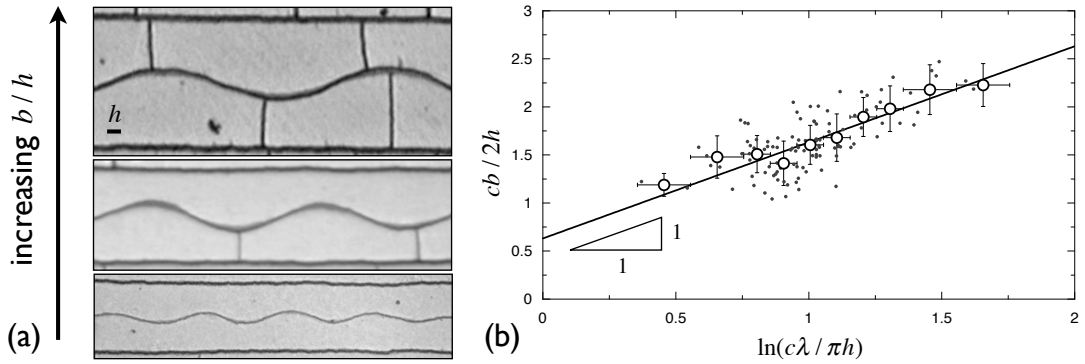

FIG. 10: (a) Wavy cracks in drying colloidal latex films form when a secondary crack tries to advance between two pre-existing straight cracks. (b) A crack path prediction that requires cracks to curve towards the direction of maximum strain energy release rate accurately predicts the relationship between wavelength λ, film thickness h, and the distance between the bounding cracks, $2b$ (for an order-1 constant c). Adapted from [6].

performed a linear stability analysis for a straight crack running between two pre-existing parallel cracks. We found that while local symmetry will predict such a crack to be stable, Eq. (31) predicts oscillations, which capably reproduce the wavelength selection of wavy cracks in drying films (see Fig. 10). However, we must conclude that this form is still noticeably incomplete in that it cannot deal with angular variations in stress [6].

A rigorous energy-based model for crack paths would allow it to fit into the emerging paradigm for other elastic instabilities – buckling, wrinkling, crinkling – in which patterns can be described by an energy balance between different modes of deformation, such as stretching and bending (*e.g.* [103–105]); fracture adds to the surface energy, at the expense of strain energy. A notably similar approach is also being followed by the group of Benoit Roman, in relation to tearing, and a review of this work appeared last year [106].

I am currently continuing my energy-based approach to understanding fracture patterns, and studying the behaviour of cracks on uneven surfaces, or in films with a non-trivial curvature.

B. Are paint cracks really elastic?

Given the applications of the fracture of paints and clays already discussed it is a fair question to ask whether they can be treated as elastic materials, or not. It is also an important applied question to ask under what conditions a film or coating will fail.

In [7, 8] I contribute to the question of when and how a colloidal film will fail. As described above, internal pore pressures can be generated during the drying of a multi-phase material, like paint or clay. These capillary pressures are the result of small menisci between the porous material's constituent particles, and act to rip the particles apart from each

other. For example, consider if solid particles are dispersed in a volatile liquid, which is then removed by evaporation. If the particles respond by assembling into a close-packed structure (as would be the equilibrium configuration of hard spheres at high-enough densities), then the final dregs of liquid will be trapped in menisci in the small pore spaces between the particles. The Young-Laplace pressures that can be supported by that fluid, before if finally evaporates, can be huge – for the colloidal silica that is used as a glossy coating for paper, the particles are of order 10 nm in diameter, and can support fluid pressures of $\sim$ 80 MPa, or about 800 atmospheres [51].

For a brittle film adhered to an unyielding substrate, a crack will grow across the film if the stress exceeds some critical stress, which depends on the thickness of the film. Since there is some maximum magnitude, p_0 to the capillary pressure, before the film dries out, one can invert this relation to predict a critical cracking thickness, below which a film will survive the rigours of drying, and above which it will break [107, 108]. For a linear elastic brittle material (and neglecting Poisson ratio effects, for demonstration purposes), this predicts that the critical film thicknesses is

$$h_c \sim \frac{G_c E}{p_0^2}. \tag{32}$$

This can explain why, for example, a thick layer of paint will crack, while a thin coat will dry smoothly. It also limits the thickness to which photonic materials can be made, by the otherwise effective method of drying [24–26].

However, many industrial paints and coatings are not linear elastic materials. A packing of spherical colloidal particles will not be expected to behave in a linear way, even if the elasticity of the material of which the particles are composed is perfectly linear. At best the particles will have Hertzian contacts, and on the length-scales of colloidal interactions these will be deformed by other forces, such as van der Waals interactions [109, 110]. Furthermore, many materials contain elements which allow for dissipation of stresses, for example by viscous flow, or creep (see *e.g.* [111] for a description of some of the complex mechanisms used). Even simple measurement of the forces at which paint cracks can be difficult. The standard method is to apply a thin film to a flexible cantilever [54, 98]. As stress develops in the film, it causes the cantilever to deflect. A suitably averaged film-stress can be then measured by monitoring the deflection of a calibrated cantilever, as in Fig. 11(a).

For [7], a collaborative paper included here, my contributions were to synthesise the colloidal polystyrene used, and developed an alternative approach to measuring stress, which involved placing a small droplet of colloid at the tip of the cantilever (Fig. 11(b)). The colloids were prepared over a range of sizes, which varied both the expected E, and p_0, of the film material. We hoped that the use of a smaller area of material would allow for a more uniform pressure to develop during drying. It did, allowing us to test some of the more recent predictions of failure criteria in non-linear elastic materials, which suggest a critical thickness that scales as $h_c \sim p_0^{-3/2}$ [54, 112], rather than that given in Eq. (32). However, the system was still quite noisy, considerably limiting the value of the tests. To develop

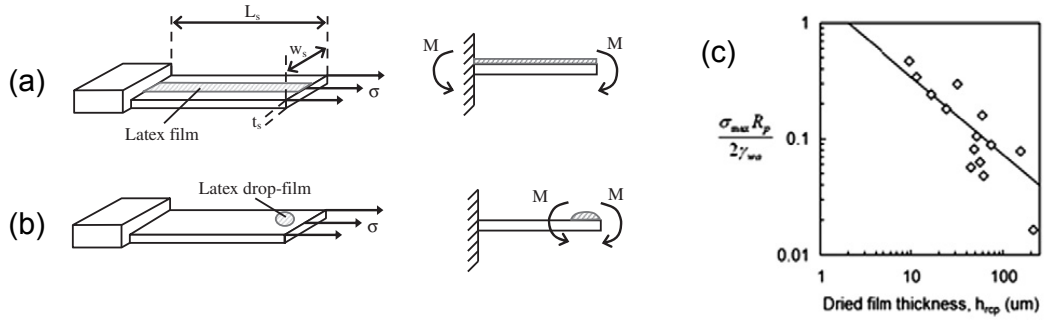

FIG. 11: (a) The deflection of a cantilever can be used to measure the stress of a film dried over it, including the stress at which fracture happens. In [7] we use this method, and (b) a droplet-based method, to look at the critical conditions for fracture, which (c) should show signatures of the non-linear elasticity of the film in the relationship of cracking stress, to film thickness. Reproduced from [7].

a better technique, which would also allow spatial resolution of stresses in the film, I was also involved in mentoring a doctoral student, in Cambridge. Together, we worked on an optical technique involving measuring interference fringes (Newton's rings), caused by the deflection of a wafer over which a drying film was cast. While successful, and now essentially complete, this research is not yet published.

In [8], the question was, rather, whether colloidal films were behaving as brittle materials. There has been a considerable amount of theoretical effort spent in either predicting the failure conditions of these films [54, 112, 113], or in analysing the results of observed deformation fields [114–117] in cracking films. In the early work that eventually led to [8] I had also been engaged in evaluating of the stress field around cracks in colloidal films, with the aim of more carefully deterimining their cracking conditions. However, the results of careful measurement of the pattern of surface deflections, as well as indentation experiments that probed the constitutive relationship of the drying colloidal materials, could not be reconciled with an elastic response, linear or not. In fact, the more precise we made the observations, and the more independent avenues of evidence we gathered, the more inconsistent the data became. For certain cases viscoelastic responses in colloidal materials are known, and exploited in order to relieve stresses gradually, rather than through fracture (e.g[111, 113]). However, the particles we were using were hard spheres, and all common wisdom suggested that the films they made were perfectly brittle, elastic bodies.

In response to this issue we began to ask the basic question of whether these films are, in fact, behaving elastically, or plastically. For this, we looked at two very different kinds of experiments. The opening width of an elastic crack, in a linear material, should follow a parabolic shape given by

$$\delta = \frac{8K_c}{E}\sqrt{r/2\pi} \tag{33}$$

for a distance r away from the crack tip [56]. We tested this prediction, and in the process

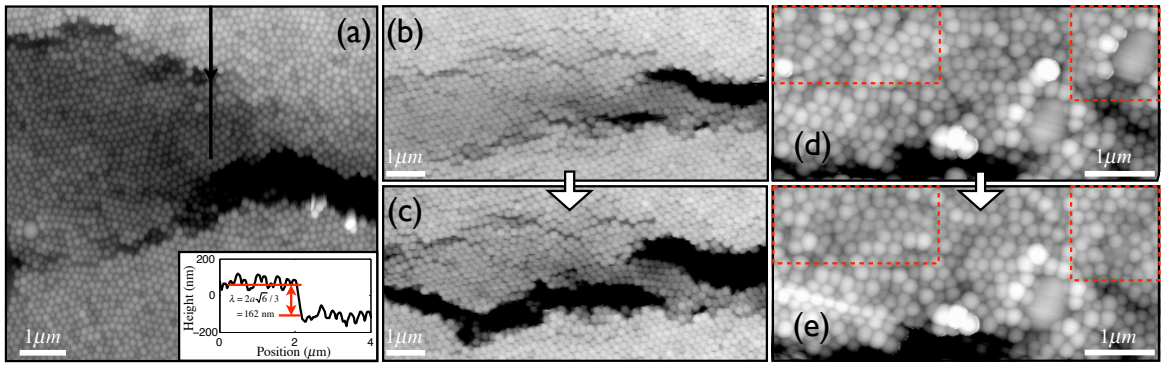

FIG. 12: Atomic force micrographs of drying latex. (a) A crack shows damage and micro-cracks ahead of the crack tip. Out-of-plane deformation is also noticed: the height profile across the overlain line segment (inset) shows a step in height of one stacking plane. (b) Another crack shows a damage zone that develops into a bridge when (c) the crack advances. The particles (d) immediately adjacent to a crack face (the black region partly seen at the bottom of the image) rearrange when (e) the crack advances. Here the dashed boxes highlight two particular areas where a large particle submerges, and where many particles rearrange. Reproduced from [8].

made quantitative measurements of the fracture toughness K_c for colloidal films. We found that paint cracks obeyed the scaling of Eq. (33). However, the values of the energy released ($G_c \simeq K_c^2$) was about an order of magnitude higher than expected from simple elastic theory, where the majority of the energy for fracture comes from creating new air-water interfaces in the broken film. We then performed simple microscope observations on drying films. A brittle, elastic crack is a reversible deformation, just like any other elastic response. If the driving forces behind it are removed, it should close. As was explained in Fig. 9 the stresses which cause fracture are the result of evaporation and Darcy flow. By blocking evaporation these stresses should disappear, and the cracks close. We performed experiments where evaporation was blocked either by a flood of water over the film, or by covering it with a glass slide. These tests showed that 20-30% of the crack opening was, indeed, reversible, but that the rest of the deformation around a crack was not. Interpreted in terms of strain energy release, this result quantitatively matched the findings of the crack tip shapes, and again suggested that only a tenth of the energy consumed in cracking went to brittle failure mechanisms. To find out where the rest of the energy was spent, atomic force microscopy was performed on drying films, *in situ*. As shown in Fig. 12 there is copious evidence for classic plastic deformation mechanisms, including the formation of dislocations, bridges, micro-cracks, as well as rearrangement of particles, around cracks drying paint films.

Finally, after identifying the mechanisms for and extent of plastic deformation, we briefly explored the implications of this finding. A simple balance of forces showed that if the yielding behaviour of the film was the result of adhesion between neighbouring particles, then plastic yielding should be ubiquitous. It also showed that plasticity should not be treated as a negative thing – and that the toughness of films should be significantly increased

by weakening the bonds between particles, to induce plastic deformation at a lower yield stress, and thereby spread any irreversible energy losses over a wider area.

VII. STRUCTURE FORMATION IN DYNAMIC DISPERSIONS

In the final section of this introduction I will explore the transport, dynamics, and structure formation during the solidification of a colloidal dispersion. This type of material is the basis of many industrial products, from traditional paints, ceramics, foodstuffs (cheeses, chocolate), as well as modern coatings, photonic materials, and composite materials. Most of the above materials begin as a liquid dispersion, which has solidified into its usable final state. During this process, significant internal stresses can develop, as already described in Section VI.B. These pressures can cause structural changes in the arrangement of the particles, as well as act as the driving force for macroscopic instabilities like fracture, buckling, or shearing, some of which have already been discussed.

Colloids also occupy an intermediate status between atomic solids, and granular materials. Their constituent particles are Brownian, and are well-described by classical thermodynamic models. However, from a quantum perspective they are macroscopic objects. They are therefore sometimes referred to as behaving like 'classical atoms'. As a model system, I am working with charged colloidal spheres. These particles interact *via* a soft Yukawa-potential, and represent one of the simplest possible steps beyond a classic hard-sphere interaction. I have shown that, generically, these materials undergo a series of transitions as they solidify (typically by drying), passing from a liquid-like state, to a repulsive colloidal glass or crystal, to an attractive colloidal solid [9, 10]. The flow of fluid during drying breaks the symmetry of the intermediate, repulsive state, and leads to a structural anisotropy of dried colloidal materials, and will result in macroscopic effects such as birefringence [11].

Much of the work presented here makes use of small-angle x-ray (SAXS) or neutron (SANS) scattering techniques. These methods use the scattering of focussed beams of radiation off interfaces in a multi-phase material, to probe that material's inner structure. This has allowed the investigation of the transitory states that occur during drying [10, 11], and the connection of these changes with macroscopic responses in dry colloidal films [11]. My expertise in these methods has also allowed me to collaborate in studying the structure of active emulsions, in an attempt to understand their propulsion mechanisms [12].

Finally, I am working on how porous granular systems, like real soils, dry. My interest in this was started by a short research project, which I pursued to follow up my doctoral studies into columnar joints, and include here. Corn starch, when dried, makes columns that look like the crack patterns in lavas. Most other granular materials don't crack in this way, and I questioned why this particular powder had such an unusual response. The results of [13] present a possible answer, which lies in the unusual distribution of pore spaces in wet starch, with water filling voids between particles, and smaller pores within starch grains.

A. Order and disorder in drying films

As a liquid dispersion dries its volatile components evaporate, and the solids slowly become more and more concentrated. For equilibrium situations these changes are simply driven by the change in free volume of the mixture, and the solvent becomes an essentially neutral background. In particular, at high enough volume fractions colloidal dispersions can organise and stiffen into colloidal crystals or glasses. A crystal structure allows for additional types of elastic response, as compared to a liquid. Since a drying material like paint or clay will pass through a range of volume fractions, it may have the opportunity to crystallise, or form into a weak repulsive solid, as it dries. However, as outlined above, in Section IV, flow of either phase can lead to additional stresses, and induce new behaviour.

The prototype for colloidal crystallisation is the equilibrium phase diagram of hard spheres, which includes a first-order phase transition from a liquid or gas-like state to a crystal. At low volume fractions a hard-sphere colloidal dispersion behaves like a fluid, with no long-range order. A solid, crystalline, phase begins to appear at a volume fraction of $\phi = 0.494$, initially in coexistence with the fluid phase. This solid-liquid co-existence continues until the dispersion reaches a volume fraction of $\phi = 0.545$, at which point the entire dispersion will have crystallised [44, 118–120]. This transition is entropically driven, as a close-packed colloidal crystal allows more room for each particle to move, and hence explore more configurations, than a random arrangement would [119, 121]. At high volume fractions the nucleation of crystals can be very slow, and the particle structure may instead resemble that of a quenched liquid, a state known as a colloidal glass [119]. In either case the particles are effectively caged by their neighbours, but can still diffuse around freely within their cages. However, the deformation of the cage structure can be anisotropic, unlike a pure liquid, and on a macroscopic scale can be described by a tensorial strain. Since the dispersion can now transmit shear stress, and has a relatively long-term structure, it has the properties of a weak, soft solid.

Charge-stabilised colloidal particles share long-range repulsive interactions and short-range attractive interactions. The standard description of these materials is Derjaguin-Landau-Verwey-Overbeek (DLVO) theory, which combines the van der Waals potential with a screened electrostatic interaction. Briefly, as a discussion of the full details of this theory can fill chapters of textbooks [14, 44], the DLVO potential between two nearby spherical colloids of radius a, and separated by a distance ℓ, can often be approximated by

$$U_D = -\frac{Aa}{12\ell} + U_0 e^{-\kappa\ell}. \tag{34}$$

Here A is the Hamaker constant, an energy scale related to the surface tension (or surface energy) of materials, and typically of order 10^{-20} J (*i.e.* a few times the thermal energy k_BT), U_0 is an electrostatic energy scale related to the surface potential of the particles, and κ^{-1} is the Debye length. This length scale can be tuned by the addition of salt, through

a range of about a nanometer, to a few tens of nanometers. For like particles the van der Waals interaction is always positive, while the electrostatic interaction is always repulsive.

In [9–11] I have begun to chart the route for solidification in a charge-stabilised colloidal dispersion. Fig. 9 has already demonstrated that when a paint or coating dries, the most common manner for this to happen is by directional solidification. This produces a gradient in pressures, and particle concentrations, from which arise differences in the structure of the drying material that sweep across the drying film as a series of fronts. This geometry means that the different behaviours of the material can be sampled by either imaging across the drying fronts at one moment, or by watching one point over time, as these fronts pass by.

The work in [9] shows that solidification should generally proceed by a two-stage process, mirroring the two different interactions of DLVO theory. As a charge-stabilised dispersion dries it will first order into a colloidal crystal or glass, which is dominated by repulsive electrostatic interactions, and then into an aggregated material, dominated by intimate van der Waals forces. Until aggregation, this process is reversible. The effect of directional drying is to spread out these two steps over a transition region of finite width, in which any set of particles stays for a finite time. For some materials these transitions in internal structure can be seen by the eye through the effects of structural colour, as shown in Fig. 13(a,b). This colour is the result of Bragg diffraction conditions being met for visible light, implies that there a regular structure on a scale of a few hundred nanometers, and can be interpreted in terms of the DLVO potentials (Fig. 13(c)).

A simple theory for this two-stage solidification should balance gradients in fluid pressure with the compression of the weak solid. The former is caused by the flow of water across the drying porous film to balance evaporation over its surface, much like a candle wick draws in wax to balance that lost to the flame. The latter effect can be related to the compressibility of the colloidal crystal, which in turn can be derived from its equation of state, or ultimately pair-wise interactions like that in Eq. (34). In [9] these interactions were varied by changing the size of the particles, and the concentration of background salt in the dispersion (and through this, the length-scale of the electrostatic interaction). We then showed how optical measurements of how things dry can be used to determine the electrostatic potential of the particles, and hence evaluate properties like their long-term stability. In other words, this work shows how colloidal stability can be evaluated with a simple microscope, rather than an expensive and dedicated instrument.

In [10], small-angle x-ray scattering (SAXS) methods were brought to bear on the topic of how paint dries. The geometry of dip-coating was chosen, both for its ease, and for its widespread industrial uses. This experiment consists of dipping a flat sheet of a wetting substrate into a liquid, and then pulling it out at a fixed speed. A thin film of liquid is left behind on the sheet, with a constant thickness that depends on the withdraw speed, and the viscosity of the liquid (see [123] for a review of this process). Similar to what is shown in Figs. 9 and 13, this film then naturally dries into a coating by directional drying. We positioned a dip-coating apparatus, filled with the colloidal silica which is used to provide

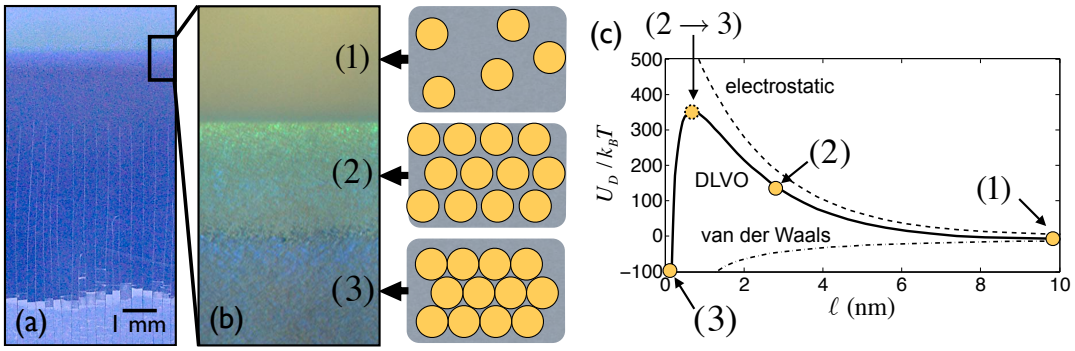

FIG. 13: Drying of a charge-stabilised colloidal dispersion. (a) Directional drying proceeds as discussed in Fig. 9, with a series of co-moving drying fronts. (b) Magnifying the liquid-solid transition region, and choosing appropriately sized particles (here 200 nm colloidal polystyrene spheres) highlights structural changes by the appearance and evolution of structural colour. The change from an opaque, milky liquid, to a green and tacky weak solid represents the nanoscopic ordering of the particles. The gradient from lime-green to dark-green shows how the particles are pushed closer towards each other, as they dry, as the inter-particle spacing changes. The jump from green to blue shows the process of aggregation, where particles jump from a repulsive state, into close contact. (c) These changes can be interpreted according to the DLVO potential of Eq. (34). For a dilute dispersion (1) there are weak interactions, and liquid-like behaviour; (2) when $U_D \sim k_B T$, the material will tend to order [44, 118, 122]. When (3) the compressive capillary forces overcome the electrostatic barrier, the particles will jump into contact, and aggregate.

gloss to paper, in the path of an x-ray beam, and observed the scattering pattern that formed off the drying dispersion.

Scattering allows precise measures of the structural information that was seen visually in [9]. While some aspects of this paper involve establishing methods for applying SAXS methods to drying colloidal dispersions – which are then exploited in [11], and elsewhere for grazing-incidence SAXS [124], or vertical SAXS [125], as well as my continuing work – it also allowed us to look carefully at the transport during drying. We showed how order arose in the sample as it dried, due to long-range repulsive interactions, and then how this order collapsed when the particles approached close enough that their polydispersity became important. This loss of order occurred during the final aggregation of the film into its final rigid form. We also tracked the motion of water and particles through the system. This showed, for example, that there was no far-field flow towards the drying front, unlike the situation for the so-called coffee-ring effect [126]. Despite the widespread uses for drying dispersions, simple basic questions such as how to predict the conditions when a flat, dry film will form, or where a flow will flow to bring the drying fluid to the edge [126] or centre [127] of a drying layer. Our contributions explore the physics of how to make a flat film.

Finally, in [11] we looked at how the ephemeral existence of the liquid-solid transition states can influence the final properties of a dried dispersion. Colloids were dried directionally in Hele-Shaw cells from which evaporation was only permitted from one open end,

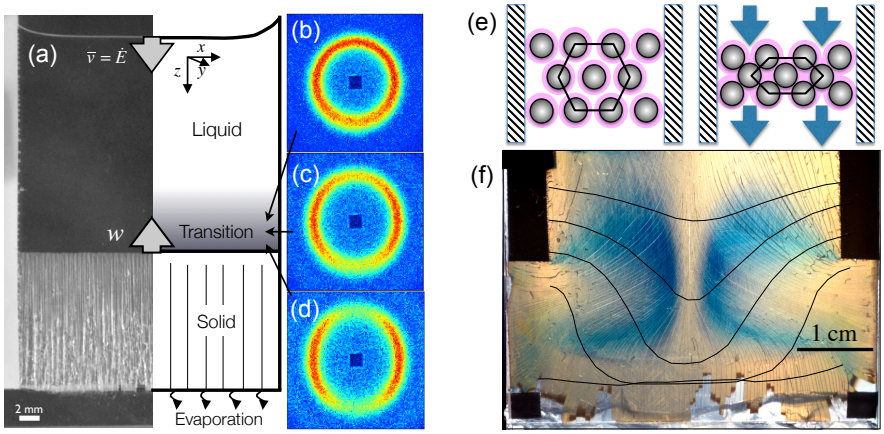

FIG. 14: (a) The directional solidification of a colloidal dispersion in a Hele-Shaw cell shows the same transition region between liquid and solid regions, as for a free-standing film. Neutron scatting patterns (b-d) across the transition region reflect the evolving arrangement of the colloidal particles, and can be used to determine the structural arrangement of the particles. (e) Once a colloidal crystal or glass forms, the flow of water through it will lead to drag forces, which compress the structure along one direction. This anisotropy is frozen in place as the dispersion aggregates and solidifies. (f) As a consequence, a dried film will appear birefringent when viewed between crossed polarisers. The pattern of birefringence follows the direction of solidification. Curves here show the position of the solidification front every 100 minutes; drying occurred from the lower edge and sides of the cell, through the gaps in the (black) spacers. Adapted from [11].

as shown in Fig. 14(a). As the material dries and solidifies the flow of water through the film breaks orientational symmetry; the dispersion is compressed, by drag forces, along the direction of water flow. Neutron scattering spectra taken across the transition from a liquid to solid (Fig. 14(b-e)) show how these drag forces lead to a structural anisotropy of the material, as sketched in Fig. 14(f). Essentially, we found that the caged colloidal particles behave as a solid until some critical yield strain, at which point they can begin to rearrange to relieve stress and strain. Curiously, the same magnitude of yield strain was measured for all the types of dispersions that were observed, despite changing the particle size, drying rate, and particle interactions *via* background salt. Even more interestingly, the yield strains exactly match those of sheared emulsions [128], suggesting that some generic geometric argument could be used to explain the magnitude of the yield strains involved.

When the dispersions finally solidify, the structural anisotropy is frozen into their final particle arrangements. This means that, on average, the particles are about ten percent closer to each other in the direction of drying, than normal to it. The effect, and its magnitude, are expected to be a robust feature of drying. In other words, these findings suggest that any paint, ceramic, or coating that is dried directionally will have an anisotropy permanently built into its basic structure, and that this anisotropy can lead to optical birefringence, mechanical instabilities like shear banding, and act to guide crack paths [11].

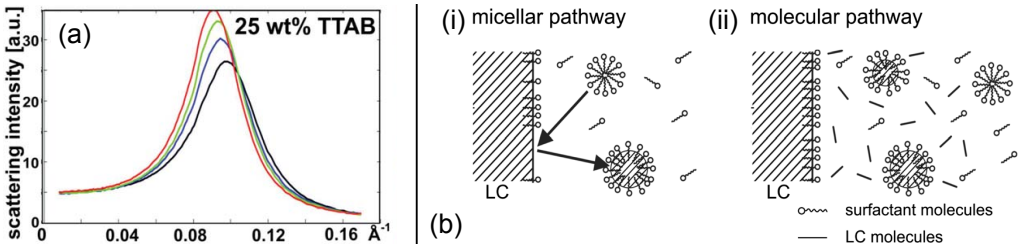

FIG. 15: Swimming droplets. (a) The scattering intensity of the equilibrium distribution of a 25 weight-% solution of TTAB with 0% (black), 1% (blue), 2% (green) and 3% (red) imply that surfactant micelles swell slightly as they absorb liquid crystal, but do not otherwise change their basic shape, or structural phase. (b) This suggests that a liquid crystal droplet swimming through a surfactant solution can interact with it by either (i) collision with empty micelles, which then fill and float away, or (ii) by the formation of a depletion zone around the drop, across which surfactant and liquid-crystal are diffusively transported. Adapted from [12].

B. Structure of active emulsions

The topic of active matter has become popular recently, both for mimicking the complex behaviour of life, and for exploring it artificially. In particular, in my institute there has been considerable attention to the topic of active emulsions, or so-called artificial swimmers (see *e.g.* [129, 130]), which can be used to explore swarming behaviour, for example. The system under study consists of a liquid crystal droplet floating in a surfactant solution. Marangoni forces on the droplet's surface can lead to an instability, and the locomotion of the droplet. This requires an imbalance of surfactant concentration on the moving droplet, and a means of sustaining this imbalance. In [12], some possible mechanisms for this are discussed.

Here, my contributions were to apply small-angle neutron-scattering methods to equilibrium mixtures of liquid crystal and surfactant in water, the results of which are shown in Fig. 15(a). The surfactant (TTAB) is present at 25% by weight, well above the critical micelle concentration. The liquid crystal is an oil phase, and virtually immiscible in water. Together, they form a micro-emulsion of oil-swollen micellar droplets, where the micelles are about 20 nm in diameter. The addition of liquid crystal stretches the micelles along one axis, by about 10% per weight-percent of liquid crystal added. This subtle change in shape proves instrumental in first determining, and then exploring, the reaction pathways along which surfactant may be lost by the droplet surface. Two such mechanisms are sketched in Fig. 15(b). These involve either (i) a population of empty micelles that collide with a swimming droplet, fill, and then transfer away a load of both liquid crystal and surfactant, or (ii) a depletion of the concentration of free surfactant (and sparingly soluble liquid crystal) molecules near the dissolving droplet, due to capture by micelles. Both can affect the surface concentration of surfactant molecules along the moving droplet. It was shown that while pathway (i) can only exert a stabilising influence, pathway (ii) can lead to continuous swimming behaviour [12].

C. Pore-scale processes and drying

The above two examples show how microscopic processes, either due to colloidal or micellar interactions, can lead to macroscopic effects. The final paper included here [13] shows how pore-scale processes are also fundamentally important to desiccation fracture patterns. It looks at how starch dries. Although many scientists have used drying starch slurries to study the formation of columnar joints [27, 67, 131, 132], there was a puzzle why the drying of this particular powder should so faithfully recreate the columnar fracture pattern, when other slurries did not. Unlike most other granular materials, or soils, there is a sharply defined drying front, similar to those discussed above in the context of colloidal dispersions, that appears when starch is dried. It is wet, un-cracked, and homogeneous to one side of this front, and broken and dry on the other side (see *e.g.* [5], Fig. 9). This sharp drying front appears to be necessary for the formation of columnar joints [28, 132].

The work in [13] starts by looking at individual starch grains, and characterising their size, and surface characteristics. It notes that each grain of starch is, itself, porous. A material made of starch grains therefore has two separate types of pore spaces: larger pores between grains, and smaller pores within grains. By combining measurements of the rheology, density, permeability and pore pressures, at different water concentrations, a clear experimental picture of how water moves through the drying starch was gathered. A detailed modelling of capillary and vapour transport in drying starch was then able to show that the presence of the two separate reservoirs of pore space allowed the pore fluid to become disconnected when there was still an unusually large amount of water left in the starch. This led to a bottleneck in the transport of moisture out of drying starch, between conditions where liquid transport was efficient, and conditions where vapour transport was efficient. The sharp drying front straddles this bottleneck in moisture transport. The unusual cracking behaviour of a starch slurry was therefore traced to the unusually porous nature of the starch grains.

While answering its specific question – why drying starch makes columns – this work also highlighted other behaviours, which may be of wider interest. One, in particular, is the non-linear elasticity of a starch block. When compressed, the starch is initially very compliant, and behaves as a material with a vanishingly small elastic modulus. As the strain reaches a few percent, the effective Young's modulus increases linearly with strain. This highly non-linear elasticity, where $\sigma \sim \epsilon^2$, can have a strong effect on the fracture conditions of granular pastes and slurries [113, 133, 134]. One projects that has begun in my group, which indirectly follows up this earlier result, is the development of an experimental model porous media consisting of glass beads held together by cured PDMS capillary bridges. These soft materials are expected to show a broad range of tuneable non-linear elastic responses.

[1] L. Goehring and S. W. Morris, *Physics Today*, 2014, **67**, 39–44.
[2] L. Goehring, *Phil. Trans. R. Soc. A*, 2013, **371**, 20120352.
[3] K. Thomas, S. Herminghaus, H. Porada and L. Goehring, *Phil. Trans. R. Soc. A*, 2013, **371**, 20120362.
[4] L. Goehring, R. Conroy, A. Akhter, W. J. Clegg and A. F. Routh, *Soft Matter*, 2010, **6**, 3562–3567.
[5] L. Goehring, *Phil. Trans. R. Soc. A*, 2013, **371**, 20120353.
[6] L. Goehring, W. J. Clegg and A. F. Routh, *Soft Matter*, 2011, **7**, 7984–7987.
[7] H. N. Yow, M. Goikoetxea, L. Goehring and A. F. Routh, *J. Colloid Interface Sci.*, 2010, **352**, 542–548.
[8] L. Goehring, W. J. Clegg and A. F. Routh, *Phys. Rev. Lett.*, 2013, **110**, 024301.
[9] L. Goehring, W. J. Clegg and A. F. Routh, *Langmuir*, 2010, **26**, 9269–9275.
[10] J. Li, B. Cabane, M. Sztucki, J. Gummel and L. Goehring, *Langmuir*, 2012, **28**, 200–208.
[11] F. Boulogne, L. Pauchard, F. Giorgiutti-Dauphiné, R. Botet, R. Schweins, M. Sztucki, J. Li, B. Cabane and L. Goehring, *Europhys. Lett.*, 2014, **105**, 38005.
[12] S. Herminghaus, C. C. Maass, C. Krüger, S. Thutupalli, L. Goehring and C. Bahr, *Soft Matter*, 2014, **10**, 7008–7022.
[13] L. Goehring, *Phys. Rev. E*, 2009, **80**, 036116.
[14] L. Goehring, S. Kitsunezaki, T. Dutta, A. Nakahara and S. Tarafdar, *Desiccation cracks and their patterns*, Wiley, 2015.
[15] Y. Couder, L. Pauchard, C. Allain, M. Adda-Bedia and S. Douady, *Eur. Phys. J. B*, 2002, **28**, 135–138.
[16] M. F. Laguna, S. Bohn and E. A. Jagla, *PLoS Comput.l Biol.*, 2008, **4**, e1000055.
[17] W. B. Zeid and D. Brutin, *Colloids Surf. A*, 2013, **430**, 1–7.
[18] W. B. Zeid, J. Vicente and D. Brutin, *Colloids Surf. A*, 2013, **432**, 139–146.
[19] K. H. Nam, I. H. Park and S. H. Ko, *Nature*, 2012, **485**, 221–224.
[20] M. C. Milinkovitch, L. Manukyan, A. Debry, N. Di-Poï, S. Martin, D. Singh, D. Lambert and M. Zwicker, *Science*, 2013, **339**, 78–81.
[21] M. A. Biot, *J. App. Phys.*, 1956, **27**, 240–253.
[22] A. Norris, *J. Appl. Phys.*, 1992, **71**, 1138–41.
[23] A. F. Routh, *Rep. Prog. Phys.*, 2013, **76**, 046603.
[24] F. Juillerat, P. Bowen and H. Hofmann, *Langmuir*, 2006, **22**, 2249–2257.
[25] J. G. McGrath, R. D. Bock, J. M. Cathcart and L. A. Lyon, *Chem. Mater.*, 2007, **19**, 1584–1591.
[26] J. Zhang, Z. Sun and B. Yang, *Curr. Opin. Colloid In.*, 2009, **14**, 103–114.
[27] G. Muller, *J. Volcanology and Geothermal Res.*, 1998, **86**, 93–96.
[28] L. Goehring, L. Mahadevan and S. W. Morris, *Proc. Nat. Acad. Sci.*, 2009, **106**, 387–392.
[29] Z. Quin, *Sci. Rep.*, 2014, **4**, 4966.
[30] A. Nakahara and Y. Matsuo, *J. Phys. Soc. Japan*, 2005, **74**, 1362–1365.
[31] D. J. Harris, H. Hu, J. C. Conrad and J. A. Lewis, *Phys. Rev. Lett.*, 2007, **98**, 148301.
[32] A. Georgiadis, A. F. Routh, M. W. Murray and J. L. Keddie, *Soft Matter*, 2011, **7**, 11098–11102.
[33] D. Brutin, B. Sobac and C. Nicloux, *J. Heat Transfer*, 2012, **134**, 061101.

[34] S. L. Bucklow, *Comp. Humanities*, 1998, **31**, 503–521.
[35] K. Yamaguchi, S. Inasawa and Y. Yamaguchi, *Phys. Chem. Chem. Phys.*, 2013, **15**, 2897–2902.
[36] S. Inasawa and Y. Yamaguchi, *Langmuir*, 2009, **25**, 11197–11201.
[37] M. A. Biot, *J. App. Phys.*, 1941, **12**, 155–164.
[38] G. J. Kynch, *Trans. Faraday Soc.*, 1952, **48**, 166–176.
[39] S. S. L. Peppin, J. A. Elliott and M. G. Worster, *Phys. Fluids*, 2005, **17**, 053301.
[40] S. S. L. Peppin, J. A. W. Elliott and M. G. Worster, *J. Fluid Mech.*, 2006, **554**, 147–166.
[41] A. M. Anderson and M. G. Worster, *Langmuir*, 2012, **28**, 16512–16523.
[42] P. Bacchin and P. Aimar, in *Nano-science: colloidal background*, ed. V. Starov, CRC Press, 2010.
[43] A. F. Routh and W. B. Russel, *AIChE J.*, 1998, **44**, 2088–2098.
[44] W. B. Russel, D. A. Saville and W. R. Schowalter, *Colloidal dispersions*, Cambridge University Press, Cambridge, 1989, p. 525.
[45] K. A. Landman and L. R. White, *AIChE J.*, 1992, **38**, 184–192.
[46] L. Pauchard, F. Elias, P. Boltenhagen, A. Cebers and J. C. Bacri, *Phys. Rev. E*, 2008, **77**, 021402.
[47] T. Khatun, M. D. Choudhury, T. Dutta and S. Tarafdar, *Phys. Rev. E*, 2012, **86**, 016114.
[48] T. Khatun, T. Dutta and S. Tarafdar, *Appl. Clay Science*, 2013, **86**, 125–128.
[49] P. C. Carman, *Trans. IChemE*, 1937, **75**, S32–S48.
[50] R. Buscall and L. R. White, *J. Chem. Soc. Faraday Trans.*, 1987, **83**, 873–891.
[51] E. R. Dufresne, D. J. Stark, N. A. Greenblatt, J. X. Cheng, J. W. Hutchinson, L. Mahadevan and D. A. Weitz, *Langmuir*, 2006, **22**, 7144–7147.
[52] J.-C. P. Gabriel, C. Sanchez and P. Davidson, *J. Phys. Chem.*, 1996, **100**, 11139–11143.
[53] H.-A. Bahr, A. Gerbatsch, U. Bahr and H.-J. Weiss, *Phys. Rev. E*, 1995, **52**, 240–243.
[54] M. S. Tirumkudulu and W. B. Russel, *Langmuir*, 2005, **21**, 4938–4948.
[55] A. A. Griffith, *Phil. Trans. R. Soc. Lond. A*, 1921, **221**, 163–198.
[56] B. R. Lawn, *Fracture of Brittle Solids*, Cambridge University Press, Cambridge, UK, 2nd edn., 1993, p. 378.
[57] M. L. Williams, *J. Appl. Mech.*, 1952, **19**, 526–528.
[58] G. R. Irwin, *J. App. Mech.*, 1957, **24**, 361–364.
[59] B. Andreotti and P. Claudin, *Phil. Trans. R. Soc. A*, 2013, **371**, 20120364.
[60] I. L'Heureux, *Phil. Trans. R. Soc. A*, 2013, **371**, 20120356.
[61] A. P. Petroff, O. Devauchelle, H. Seyblod and D. H. Rothman, *Phil. Trans. R. Soc. A*, 2013, **371**, 20120365.
[62] C. D. Lio, A. D'Alpaos and M. Marani, *Phil. Trans. R. Soc. A*, 2013, **371**, 20120367.
[63] M. Wells and R. Cossu, *Phil. Trans. R. Soc. A*, 2013, **371**, 20120366.
[64] G. Penny, K. Daniels and S. Thompson, *Phil. Trans. R. Soc. A*, 2013, **371**, 20120359.
[65] Y. Zelnik, S. Kinast, H. Yizhaq, G. Bel and E. Meron, *Phil. Trans. R. Soc. A*, 2013, **371**, 20120358.
[66] B. Hallet, *Phil. Trans. R. Soc. A*, 2013, **371**, 20120357.
[67] L. Goehring and S. W. Morris, *Europhys. Lett.*, 2005, **69**, 739–745.
[68] L. Goehring, Z. Lin and S. W. Morris, *Phys. Rev. E*, 2006, **74**, 036115.
[69] L. Goehring and S. Morris, *J. Geophys. Res.*, 2008, **113**, B10203.
[70] N. Noffke, R. Hazen and N. Nhleko, *Geology*, 2003, **31**, 673–676.
[71] H. Porada, J. Ghergut and E. Bouougri, *Palaios*, 2008, **23**, 65–77.

[72] C. D. Walcott, *Smithsonian Misc. Coll.*, 1914, **64**, 77–156.
[73] J. Hagadorn and D. Bottjer, *Geology*, 1997, **25**, 1047–1050.
[74] G. Gerdes, in *Atlas of microbial mat features preserved within the clastic rock record*, ed. J. Schieber, P. Bose, P. Eriksson, S. Banjeree, S. Sarkar, W. Altermann and C. O., Elsevier, 2007, pp. 5–38.
[75] J. N. Wilking, T. E. Angelini, A. Seminara, M. P. Brenner and D. A. Weitz, *MRS Bull.*, 2011, **36**, 385–391.
[76] T. Shaw, M. Winston, C. Rupp, I. Klapper and P. Stoodley, *Phys. Rev. Lett.*, 2004, **93**, 098102.
[77] G. Mariotti, S. B. Pruss, J. T. Perron and T. Bosak, *Nature Geoscience*, 2014, **7**, 736–740.
[78] A. H. Lachenbruch, *U. S. Geol. Surv. Spec. Paper*, 1962, **70**, 69.
[79] J. R. Mackay, *Can. J. Earth Sci.*, 1974, **11**, 1366–1383.
[80] M. T. Mellon, C. P. Mckay and J. L. Heldmann, *Antarctic Sci.*, 2014, **26**, 413–426.
[81] T. Bai, D. D. Pollard and H. Gao, *Nature*, 2000, **403**, 753–756.
[82] T. E. Berg and R. F. Black, in *Antarctic soils and soil forming processes*, ed. J. C. F. Tedrow, Am. Geophys. Union, 1966, pp. 61–108.
[83] R. S. Sletten, B. Hallet and R. C. Fletcher, *J. Geophys. Res.*, 2003, **108**, 8044.
[84] S. Bohn, L. Pauchard and Y. Couder, *Phys. Rev. E*, 2005, **71**, 046214.
[85] J. R. Mackay, *Can. J. Earth Sci.*, 1993, **30**, 509–518.
[86] G. V. Chavdarian and D. Y. Sumner, *Sedimentology*, 2010, **58**, 407–423.
[87] E. Bouchbinder, J. Fineberg and M. Marder, *Annu. Rev. Condens. Matter Phys.*, 2010, **1**, 1–25.
[88] M. Sendova and K. Willis, *Appl. Phys. A*, 2003, **76**, 957–959.
[89] V. Lazarus and L. Pauchard, *Soft Matter*, 2011, **7**, 2552.
[90] D. Vella, H.-Y. Kim, P. Aussillous and L. Mahadevan, *Phys. Rev. Lett.*, 2006, **96**, 178301.
[91] J. Bostwick and K. Daniels, *Phys. Rev. E*, 2013, **88**, 042410.
[92] G. Gauthier, V. Lazarus and L. Pauchard, *Langmuir*, 2007, **23**, 4715–4718.
[93] M. Fender, F. Lechenault and K. Daniels, *Phys. Rev. Lett.*, 2010, **105**, 125505.
[94] B. Cotterell and J. R. Rice, *Int. Jour. Frac.*, 1980, **16**, 155–169.
[95] B. Cotterell, *Int. Jour. Frac. Mech.*, 1965, **1**, 96–103.
[96] Y. Matsuo and A. Nakahara, *J. Phys. Soc. Japan*, 2012, **81**, 024801.
[97] R. C. Chiu, T. J. Garino and M. J. Cima, *J. Am. Ceram. Soc.*, 1993, **76**, 2257–64.
[98] R. C. Chiu and M. J. Cima, *J. Am. Ceram. Soc.*, 1993, **76**, 2769–77.
[99] C. Allain and L. Limat, *Phys. Rev. Lett.*, 1995, **74**, 2981–2984.
[100] K. A. Shorlin, J. R. de Bruyn, M. Graham and S. W. Morris, *Phys. Rev. E.*, 2000, **61**, 6950.
[101] L. Pauchard, M. Adda-Bedia, C. Allain and Y. Couder, *Phys. Rev. E*, 2003, **67**, 027103.
[102] J. A. Hodgdon and J. P. Sethna, *Phys. Rev. B*, 1993, **47**, 4831–4840.
[103] B. Li, Y.-P. Cao, X.-Q. Feng and H. Gao, *Soft Matter*, 2012, **8**, 5728.
[104] P. Kim, M. Abkarian and H. A. Stone, *Nature Materials*, 2011, **10**, 952–957.
[105] P. M. Reis, F. Corson, A. Boudaoud and B. Roman, *Phys. Rev. Lett.*, 2011, **103**, 045501.
[106] B. Roman, *Int. J. Fract.*, 2013, **182**, 209–237.
[107] J. L. Beuth Jr., *Int. J. Solids Structures*, 1992, **29**, 1657–1675.
[108] J. W. Hutchinson and Z. Suo, *Adv. Appl. Mech.*, 1992, **29**, 63–191.
[109] K. Johnson, K. Kendall and A. D. Roberts, *Proc. R. Soc. London Ser A*, 1971, **324**, 301–313.
[110] K. Kendall, N. M. Alford and J. D. Birchall, *Proc. R. Soc. Lond. A*, 1987, **412**, 269–283.
[111] A. F. Routh and W. B. Russel, *Langmuir*, 1999, **15**, 7762–7773.

[112] K. Singh and M. Tirumkudulu, *Phys. Rev. Lett.*, 2007, **98**, 218302.
[113] W. Man, N. Wu and W. B. Russel, *Langmuir*, 2008, **24**, 1721–1730.
[114] J. Zarzycki, *J. Non-crystalline Solids*, 1988, **100**, 359–363.
[115] Y. Xu, W. C. Engl, E. R. Jerison, K. J. Wallenstein, C. Hyland, L. A. Wilen and E. R. Dufresne, *Proc. Nat. Acad. Sci.*, 2010, **107**, 14964–14967.
[116] G. Gauthier, V. Lazarus and L. Pauchard, *Europhys. Lett.*, 2010, **89**, 26002.
[117] A. Sarkar and M. S. Tirumkudulu, *Soft Matter*, 2011, **7**, 8816–8822.
[118] S. Hachisu and Y. Kobayashi, *J. Colloid Interface Sci.*, 1974, **46**, 470–476.
[119] P. N. Pusey and W. van Megen, *Nature*, 1986, **320**, 340–342.
[120] Z. Cheng, P. M. Chaikin, W. B. Russel, W. V. Meyer, J. Zhu, R. B. Rogers and R. H. Ottewill, *Materials and Design*, 2001, **22**, 529–534.
[121] W. B. Russel, *Nature*, 2003, **421**, 490–491.
[122] A. Kose, M. Ozaka, K. Takano, Y. Kobayashi and S. Hachisu, *J. Colloid Interface Sci.*, 1973, **44**, 330–338.
[123] M. Maleki, M. Reyssat, F. Restagno, D. Quéré and C. Clanet, *J. Colloid Interface Sci.*, 2011, **354**, 359–363.
[124] J. Perlich, M. Schwartzkopf, V. Körstgens, D. Erb, J. F. H. Risch, P. Müller-Buschbaum, R. Röhlsberger, S. V. Roth, and R. Gehrke, *Phys. Status Solidi RRL*, 2012, **6**, 253–255.
[125] S. Kim, K. Hyun, Y. S. Kim, B. Struth, C. Clasen, and K. H. Ahn, *Langmuir*, 2012, **29**, 10059–10065.
[126] R. D. Deegan, O. Bakajin, T. F. Dupont, G. Huber, S. R. Nagel and T. A. Witten, *Nature*, 1997, **389**, 827–829.
[127] K. A. Baldwin, M. Granjard, D. I. Willmer, K. Sefiane and D. J. Fairhurst, *Soft Matter*, 2011, **7**, 7819.
[128] T. T. Mason, J. Bibette and D. A. Weitz, *J. Colloid Interface Sci.*, 1996, **179**, 439–448.
[129] S. Thutupalli, R. Seemann and S. Herminghaus, *New J. Phys.*, 2011, **13**, 073021.
[130] S. Thutupalli and S. Herminghaus, *Eur. Phys. J. E*, 2013, **36**, 91–100.
[131] A. Toramaru and T. Matsumoto, *J. Geophys. Res.*, 2004, **109**, B02205.
[132] T. Mizuguchi, A. Nishimoto, S. Kitsunezaki, Y. Yamazaki and I. Aoki, *Phys. Rev. E*, 2005, **71**, 056122.
[133] S. Kitsunezaki, *Phys. REv. E*, 2013, **87**, 052805.
[134] W. Man and W. B. Russel, *Phys. Rev. Lett.*, 2008, **100**, 198302.

VIII. LIST OF INCLUDED PUBLICATIONS

1. **L. Goehring** and S. W. Morris., Cracking mud, freezing dirt and breaking rocks, Physics Today, November 2014, 39-44.

2. **L. Goehring**, Pattern formation in the geosciences, Philosophical Transactions of the Royal Society A 371 20120352 (2013).

3. K. Thomas, S. Herminghaus, H. Porada, and **L. Goehring**, Formation of Kinneyia via shear-induced instabilities in microbial mats, Philosophical Transactions of the Royal Society A 371 20120362 (2013).

4. **L. Goehring**, R. Conroy, and A. Akhter, W. J. Clegg, and A. F. Routh. Evolution of mud-crack patterns during repeated drying cycles. Soft Matter, 6, 3562 (2010).

5. **L. Goehring**, Evolving fracture patterns: columnar joints, mud cracks and polygonal terrain, Philosophical Transactions of the Royal Society A, 371, 20120353 (2013).

6. **L. Goehring**, W. J. Clegg, and A. F. Routh. Wavy cracks in drying colloidal films. Soft Matter, 7, 7984-7987 (2011).

7. H. N. Yow, M. Goikoetxea, **L. Goehring**, and A. F. Routh. Effect of film thickness and particle size on cracking stress in drying latex films. Journal of Colloid and Interface Science 352, 542-548 (2010).

8. **L. Goehring**, W. J. Clegg, and A. F. Routh, Plasticity and Fracture in drying colloidal films, Physical Review Letters 110, 024301 (2013)

9. **L. Goehring**, W. J. Clegg, and A. F. Routh. Solidification, ordering, and aggregation of a drying colloidal dispersion. Langmuir, 26, 9269-9275 (2010).

10. J. Li, B. Cabane, M. Sztucki, J. Gummel, and **L. Goehring**, Drying Dip-Coated Colloidal Films, Langmuir, 28, 200-208 (2012).

11. F. Boulogne, L. Pauchard, F. Giorgiutti-Dauphin, R. Botet, R. Schweins, M. Sztucki, J. Li, B. Cabane, and **L. Goehring**, Structural anisotropy of directionally dried colloids, Europhysics Letters 105, 38005 (2014).

12. S. Herminghaus, C. C. Maass, C. Krger, S. Thutupalli, **L. Goehring**, and C. Bahr, Interfacial mechanisms in active emulsions, Soft Matter 10, 7008-7022 (2014).

13. **L. Goehring**. Drying and cracking mechanisms in a starch slurry. Physical Review E 80, 036116 (2009).